AD-A043 041 PURDUE UNIV LAFAYETTE IND PROJECT SQUID HEADQUARTERS F/G 20/4
TURBULENCE MEASUREMENTS OF A TWO-DIMENSIONAL HELIUM JET IN A MO--ETC(U)
JUL 77 P ANDERSON, J C LARUE, P A LIBBY N00014-75-C-1143

UNCLASSIFIED SQUID-UCSD-9-PU NL

| OF |
ADA043041

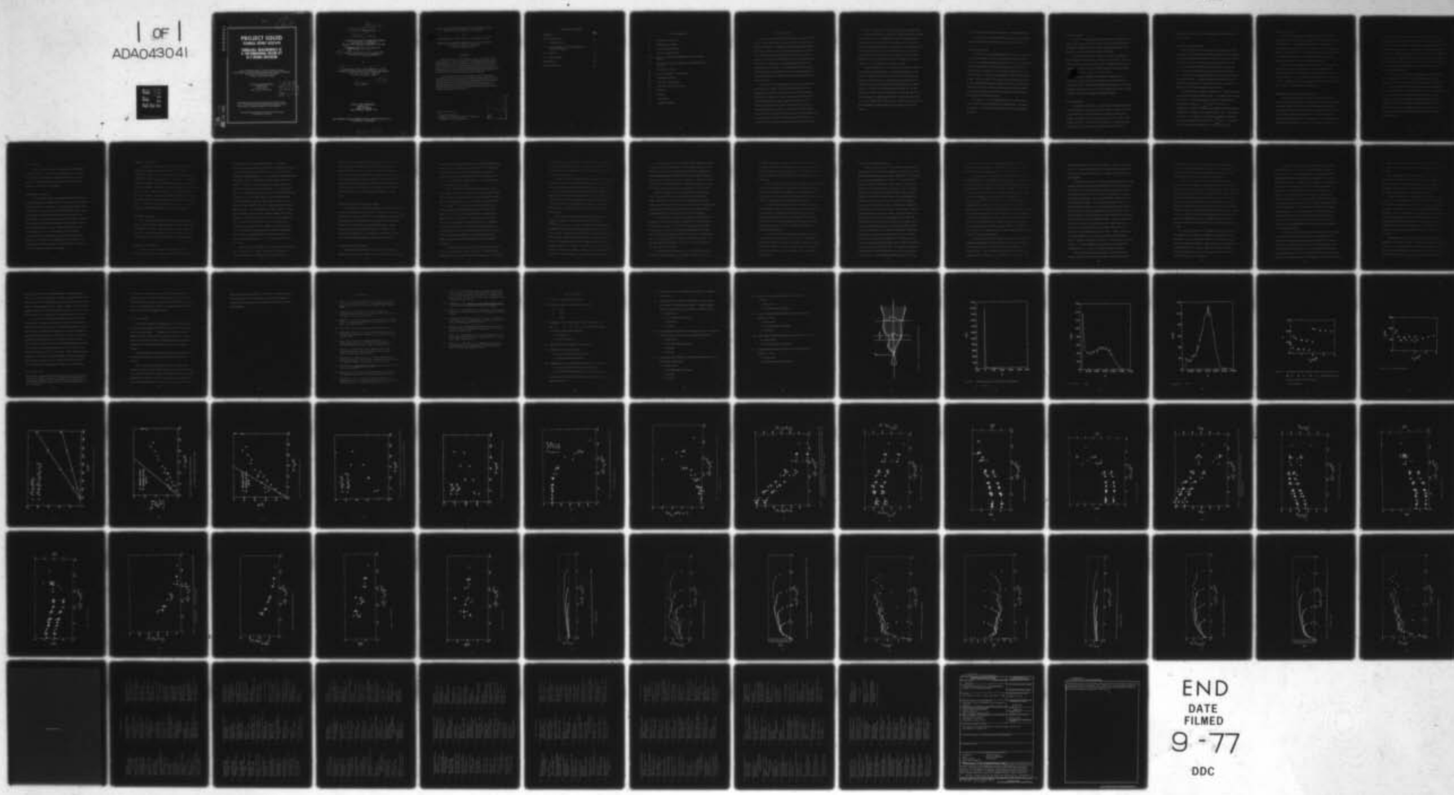

END
DATE
FILMED
9-77
DDC

PROJECT SQUID

TECHNICAL REPORT UCSD-9-PU

TURBULENCE MEASUREMENTS OF A TWO-DIMENSIONAL HELIUM JET IN A MOVING AIRSTREAM

by

PAUL ANDERSON, JOHN C. LARUE, AND PAUL A. LIBBY
DEPARTMENT OF APPLIED MECHANICS AND ENGINEERING SCIENCES
UNIVERSITY OF CALIFORNIA, SAN DIEGO
LA JOLLA, CALIFORNIA 92093

PROJECT SQUID HEADQUARTERS
CHAFFEE HALL
PURDUE UNIVERSITY
WEST LAFAYETTE, INDIANA 47907

Project SQUID is a cooperative program of basic research relating to Jet Propulsion. It is sponsored by the Office of Naval Research and is administered by Purdue University through Contract N00014-75-C-1143, NR-098-038.

9

14 SQUID-

Technical Report UCSD-9-PU

PROJECT SQUID

A COOPERATIVE PROGRAM OF FUNDAMENTAL RESEARCH
AS RELATED TO JET PROPULSION
OFFICE OF NAVAL RESEARCH, DEPARTMENT OF THE NAVY

15 ~~CONTRACT~~ NØØ14-75-C-1143 NR-098-038

6

TURBULENCE MEASUREMENTS OF A TWO-DIMENSIONAL HELIUM JET IN A MOVING AIRSTREAM.

by

10

Paul Anderson, John C. LaRue, and Paul A. Libby
Department of Applied Mechanics and Engineering Sciences
University of California, San Diego
La Jolla, California 92093

12 69p.

11 July 1977

PROJECT SQUID HEADQUARTERS
CHAFFEE HALL
PURDUE UNIVERSITY
WEST LAFAYETTE, INDIANA 47907

403 617

LB

TURBULENCE MEASUREMENTS OF A TWO-DIMENSIONAL HELIUM JET IN A MOVING AIRSTREAM

by

Paul Anderson,* John C. LaRue,** and Paul A. Libby***

Department of Applied Mechanics and Engineering Sciences
University of California, San Diego
La Jolla, California 92093

ABSTRACT

Measurements of the streamwise velocity component and the concentration of helium are made in a two-dimensional helium jet discharging into a moving airstream. The transverse distribution of the unconditioned and conditioned statistics of the velocity and helium concentration at various downstream positions are presented. In addition range conditioned point statistics provide information on the structure of turbulent zones of various durations.

The gross properties of the jet agree with previous data. Entrainment is found to occur on the leeward edges of the turbulent zones; because the turbulent fluid is moving faster than the external stream these edges are on the upstream end of the zones. The interfaces as given by the velocity and concentration cannot be distinguished and are found to be relatively thicker than previously measured temperature interfaces.

---

* Research Assistant.
** Assistant Research Engineer and Lecturer.
*** Professor of Fluid Mechanics.

TABLE OF CONTENTS

LIST OF SYMBOLS

x	downstream coordinate
y	transverse coordinate
X	hot film voltage squared
Y	hot wire voltage squared
$\overline{u}, u'$	mean and fluctuating components of the streamwise velocity
$\overline{c}, c'$	mean and fluctuating components of the helium mass fraction
U_∞	free stream velocity
x_o	location of apparent virtual origin
θ	momentum thickness
$\overline{u}_o$	centerline mean velocity
$\overline{c}_o$	centerline mean concentration
S	skewness
K	kurtosis
γ	intermittency
f_γ	crossing frequency

I. INTRODUCTION

It is widely recognized that measurements of passive scalars provide valuable information on the properties of turbulent shear flows. Accordingly, it is somewhat surprising that there appear to be no data on passive scalars in the fundamentally important flow which results from a two-dimensional jet issuing into a moving stream. In this paper we present data on the streamwise velocity and helium concentration in a two-dimensional helium jet discharging into an airstream. The measurements are sufficiently downstream from the exit plane of the jet so that only small concentrations of helium are involved and so that the helium may be treated as passive.

The velocity in two-dimensional jets in a moving stream has been widely investigated. Rodi[1] provides a valuable critical assessment of available velocity data on a variety of low-speed turbulent shear flows; with respect to the two-dimensional jet in the moving stream he cites the results of Weinstein et al.,[2] Bradbury and Riley,[3] and Everitt[4] but concludes that there are no measurements sufficiently far downstream so that flow similarity is achieved. Relative to a different flow, the two-dimensional jet discharging into a quiescent ambient, Kotsovinos[5] observes recently that the discrepancy among the data for such jets can be

Rodi[1] concludes that no available data on the two-dimensional jet in a moving stream have extended far enough downstream to apply to this third region. In attempting to reduce our measurements to similarity form, we find that in several respects our data do not agree with their well known wake counterparts; we refer particularly to the gross behavior associated with the decay of the centerline velocity and with the growth of the half-velocity location. Other quantities which involve normalization with respect to centerline values, e.g., are comparable to far-wake results.

Despite the absence of strict similarity, we find it convenient for purposes of data presentation to identify an apparent virtual origin, recognizing that this is not the correct virtual origin for the third, far-field region. The momentum thickness, which is constant in wakes and jets provided the external flow has constant velocity, is used as a non-dimensionalizing length; for our case in which the initial velocity of the helium is higher than that in the moving stream, the appropriate definition of momentum thickness is $\theta = 2\int_0^\infty (\bar{\rho}/\rho_\infty)(\bar{u}/U_\infty)\left((\bar{u}/U_\infty) - 1\right) dy$ where the overbar denotes the usual time-averaged quantity and the notation is clear from Figure 1.

II. ARRANGEMENT AND TECHNIQUES OF THE EXPERIMENT

In this section we describe the flow conditions and the experimental and data reduction techniques used in the present work.

Description of the flow

A symmetric, airfoil shaped tube with a chord of 5.14 cm and a maximum thickness of 2.18 cm is mounted across the working section of a low-speed wind tunnel having a 76 × 76 cm cross section. Helium is injected at the trailing edge of the tube from a line of uniform holes of diameter 1.59 mm and with a spacing of 0.254 cm between centers. The helium is supplied by a bank of high pressure bottles, heated to within 1.5°C of the airstream temperature prior to being introduced at both ends of the airfoil tube, and distributed within the airfoil by a perforated inner tube of 9.52 mm diameter. A temperature probe at one end of the airfoil provides the sensor for the control of the helium heater.

The velocity, U_∞, and turbulence level in the free stream are 4.6 ± 0.06 m/s and less than 0.07% respectively. The initial jet velocity U_j is about 85 m/s as estimated from the momentum thickness.

Probe and Support

Velocity and concentration measurements are made with a two-sensor probe similar to that described in Way and Libby[6] and LaRue and Libby.[7] Briefly, the probe consists of a hot film normal to the flow and a hot-wire in the thermal field of the film.

A standard height gauge, resting on the floor of the tunnel, is used to support the probe to an accuracy of $2.5(10)^{-2}$ mm. Vertical traverses across the jet are made at four streamwise locations corresponding to values of the x-coordinate measured from the trailing edge of the tube of $x = 43$, 87, 131, and 174 cm.

The frequency response of the probe is estimated to be at least 500 Hz on the basis of measurements on a similar probe by LaRue and Libby.[7] The spatial resolution corresponds to a rectangle normal to the flow of 0.25×0.5 mm; the longest side of the rectangle is about 3-4 times the estimated Kolmogoroff length.

Probe Calibration

The probe is calibrated in a calibration jet installed temporarily in the wind tunnel at velocities within the expected range of velocities in the turbulent jet, namely from four to twelve m/s and at five helium-air mixtures with helium mass fractions of 0, 0.019, 0.049, 0.087, and 0.203. The calibration techniques are essentially those described in LaRue and Libby[7] and Stanford and Libby[8] for the determination of u-c pairs from a digital pair of voltages from the film and wire.

Data Collection and Reduction

Both calibration and turbulent data are processed by an ADC having twelve bit resolution and recorded on digital tape at a sample rate of 2086 samples per second per channel. At each probe position 30 seconds of data are recorded; for the unconditioned and zone averages presented here only ten seconds of data are used, but range conditioned, point statistics require all thirty seconds of data in order to obtain adequate statistics even for the mean values and lowest moments. To make possible future data reduction, the signals from the sensors and their derivatives are recorded on a Honeywell 7610 FM instrumentation tape at 15 ips.

Consider the data reduction technique; let X denote the square of the voltage from the normal film and Y the square of the voltage from the wire. The mass fraction of helium is obtained from a polynomial of the form $c = \sum_{n=0}^{n=2} A_n(Y) X^n$ where the A_n coefficients are taken to be third-order polynomials in the indicated variable and are based on the calibration data. With c determined for a X-Y pair of voltages, the u-velocity component is obtained from another polynomial of the form $X = \sum_{n=0}^{n=2} B_n(c) u^n$ where the B_n are second order polynomials in the indicated variable.

Measures of Accuracy

As part of the assessment of experimental errors, measurements are made to determine the sensitivity of the probe to variations in temperature. It is found that at low helium concentrations and at velocities up to about five m/s a two-degree change in temperature leads to errors of $3(10)^{-3}$ in concentration and of 20 cm/s in velocity. Accordingly, as noted earlier, the temperature of the helium is maintained within $1.5^{\circ}C$ of the airstream temperature.

Known values of velocity and concentration for the calibration data provide a means of evaluating the error in the polynomial inversion schemes. Calibration data corresponding to $4.0 \text{ m/s} \leq u \leq 8.0 \text{ m/s}$ and $0.0 \leq c \leq 0.05$ result in maximum mean and RMS errors of $\pm$ 0.07 m/s and $\pm$ 0.05 m/s respectively for velocity and $\pm 6(10)^{-4}$ and $\pm 8(10)^{-4}$ respectively for concentration.

Determination of the Intermittency Function

The helium concentration is used to discriminate between turbulent and irrotational fluid. Although the wind tunnel is operated in an open fashion, a slight increase in the background helium concentration is detected by the probe during successive measurements at each downstream measuring station. Figures 2a-c show the probability density function for concentration at various downstream and transverse locations. The peak of the spike on the left of each distribution is taken as the level of the helium in the external flow due to contamination. The thickness of the spike is associated with a variety of effects: experimental inaccuracies, spurious fluctuations in helium concentration in the external flow, and contributions from the interfaces between turbulent and irrotational fluid. Our explanation for the increase in apparent helium concentration in the external flow is consistent with the observed increase in the peak value of the pdf's at a given downstream measuring station as the probe is moved sequentially through the jet.

In Figures 3a-b we indicate the influence on the intermittency and crossing frequencies of various increments above the peak value. We note that at probe positions corresponding to values of $\gamma < 0.5$ a low threshold value increases the apparent intermittency and crossing frequency while in regions of $\gamma > 0.50$ a low threshold value increases the intermittency and decreases the crossing frequency. On the basis of these variations we have selected a threshold 0.001 greater than the peak value as indicated by the shaded symbols. Note that these values are in the range of c_T in which the intermittency and crossing frequency are relatively insensitive to c_T.

III. RESULTS

In this section we compare our results for the development of the jet with earlier experiments and then present our results in terms of unconditioned and conditioned statistics. First the location of the fluid-dynamic centerline and the location of the apparent virtual origin are discussed.

Fluid-dynamic Centerline

The y-coordinate used in our data presentation relates to the normal distance from a fluid mechanical centerline which can deviate from the geometric centerline due to slight buoyancy effects; these are expected to arise in an intermediate downstream location where the maximum velocity and maximum helium concentration are diminishing. In fact we find the corrections to be small. Nevertheless the location of the fluid mechanical centerline and the values of the maximum velocity, $u_o(x)$, and of the maximum helium concentration, $c_o(x)$, are determined at each streamwise location by fitting in a least square sense a parabola through at least five sets of data in the neighborhood of the centerline. We find offsets of the fluid mechanical centerline from 5.5 mm above to 1.8 mm below the geometric centerline.

Apparent Virtual Origin

The apparent virtual origin for the flow is calculated by assuming a similarity profile of the form $(\bar{u} - U_\infty)/(\bar{u}_o - U_\infty) = \exp\left(-\alpha y^2/(x - x_o)\right)$. At each downstream location the values of $-y^2/\left(\ln(\bar{u} - U_\infty)/(\bar{u}_o - U_\infty)\right)$, where y, $\bar{u}$, and U_∞ are measured quantities and where $\bar{u}_o$ is computed as part of the determination of the fluid-dynamic centerline, are averaged and plotted as a function of x. Likewise a similarity profile for $\bar{c}$ is assumed and the procedure repeated. A least square approximation of the resulting distribution shown in Figure 4 leads to a virtual origin for velocity at $x_o = 17.8$ cm and for concentration at $x_o = 16.0$ cm. These apparent virtual origins are used in the data presentation.

Momentum Thickness

The momentum thickness, used as a non-dimensionalizing length, is determined by graphically integrating smoothed profiles of $(\rho/\rho_\infty)(\bar{u}/U_\infty)\left((\bar{u}/U_\infty) - 1\right)$ across the jet at each downstream location. All of the stations yield values of θ within 16% of an average value of 7.1 cm, which is used in the data presentation.

Downstream Development

In Figures 5a-b we compare our results on gross jet behavior with earlier measurements and with the theory of wakes and jets based on far-field approximations. The standard presentation of gross behavior involves the variation with $(x - x_{ou})/\theta$ of the centerline velocity in the form $\left(U_\infty/(u_o - U_\infty)\right)^2$ and the variation of the half-width, i.e., the value of the y-coordinate where the velocity excess is one-half its centerline value, in the form $(\delta_{\frac{1}{2}}/\theta)^2$. In Figure 5a - b we compare our results with those of Weinstein et al.[2] and of Bradbury and Riley.[3] The three sets of data are in reasonable agreement within the context of the sensitivity of jet data to a variety of flow effects. We also show on these figures the theory for the far field of wakes and jets (cf., e.g., Schlichting[9] and Libby[10]) based on the experimentally determined apparent origin. The considerable discrepancy is noted. Thus as indicated earlier we have another example of apparent but faulty similarity. We note that in order to bring our experimental data into accord with the far-field theory we would require an unreasonable x_{ou}, namely 53 cm. Finally, we note that in order for us to obtain farther downstream data without compromising excessively the two-dimensionality of the jet would require a reduced momentum thickness, i.e., a reduced initial velocity at the jet exit.

In Figures 6a-b we compare the gross behavior of the velocity and concentration. The mean concentration of helium on the centerline decays more rapidly and the half-width based on a mean helium concentration equal to one half its centerline value is found to grow more rapidly than the corresponding quantities associated with the velocity. These are expected results, now understood to be associated with the relatively high level of a scalar in the turbulent fluid far from the centerline. The difference in the behavior of the two quantities, velocity and scalar concentration, is undoubtedly due to the influence of the pressure on the former and to the absence of a corresponding distributing force on the latter.

Intermittency Factor and Crossing Frequency

The distributions of the intermittency factor and of the crossing frequency are shown in Figures 7 and 8. The peak in the crossing frequency near $y/\left((x - x_o)\theta\right)^{\frac{1}{2}} = 0.32$ corresponds to the $y/((x-x_o)\theta)^{\frac{1}{2}}$ location where the intermittency factor equals 0.50, as generally expected. Note that we have non-dimensionalized the crossing frequency so as to form a Strouhal number by introducing the characteristic length and U_∞; the resulting correlation of the data from various streamwise stations is considered satisfactory.

Unconditioned and Zone Statistics

Unconditioned and turbulent zone mean, root mean square, skewness and kurtosis distributions for the velocity and concentration are shown in Figures 9a-d and 10a-d, where symbols representing quantities in the turbulent zones are flagged. The corresponding data for the velocity in the non-turbulent zones are shown in Figures 11a-d. Here we adopt the notation of Kovaszany et al.,[11] $(\sim)$ for a turbulent zone average, and $(\sim)$ for a non-turbulent, i.e., irrotational, zone average.

We discuss some of the interesting results shown in this large number of figures. Consider first the distributions of mean velocity: Figure 9a indicates that the turbulent fluid moves faster than the external airstream. In fact except for one data point at $y\left((x - x_{ou})\theta^{-\frac{1}{2}}\right) = 0.43$, which may be in slight error, the velocity within the turbulent fluid at the edge of the jet moves faster than U_∞ with an increment of about five percent of the maximum velocity difference. Close to the jet centerline the velocity in the irrotational zones is higher than U_∞, suggesting that the turbulent fluid carries along the air between the large turbulent structures. Near the outer edges of the jet, the velocity in the irrotational fluid appears to be somewhat less than U_∞, consistent with motion of the external flow over the turbulent structures.

The view which emerges from these velocity distributions is in accord with that given by Kovaszany et al.[11] for the turbulent boundary layer and by Fabris[12] for the turbulent wake of a cylinder.

In both of these previous cases the turbulent fluid moves slower than the external flow so that behavior is reversed but is qualitatively consistent with our results in which the turbulent fluid moves faster than the external stream.

Consider next the distributions of the mean helium concentration as shown in Figure 10a. Of particular interest is the relatively high value for the average within the turbulent fluid near the edges of the jet. In fact the concentration within the turbulent fluid appears to approach a constant value of about 40% of the centerline mean at the outer edge; this is in agreement with the results of Fabris[12] and of LaRue and Libby[14] for the temperature in the wake of a heated cylinder and is in contrast with the behavior of the zone averaged mean velocity.

Figure 9b and 11b indicate the data on the intensity of the velocity fluctuations. On the centerline of the jet we find $\left(\overline{(u'^2)}^{\frac{1}{2}} / (\bar{u}_o - U_\infty) \right) = 0.27$. There is considerable variation among the published values for this relative intensity on the centerline of wakes and jets. Bradbury and Riley[3] indicate that this value increases as the far-field is approached and becomes in reasonable agreement with the corresponding value given by Townsend for the wake of a cylinder, namely 0.25. However, Fabris[12] gives 0.20 for this same quantity in the wake of a cylinder. Thus, while our value is somewhat high, it is not inconsistent with previous measurements.

The distributions of relative intensity of the velocity fluctuations across the jet have the expected behavior; the peak intensity occurs off-axis but in the region of the jet with almost fully turbulent flow. The intensity within the turbulent fluid at the outer edge of the jet as a percent of centerline value is high, roughly 65%. Also the intensity of the velocity fluctuations within the irrotational zones in the middle of the jet is also high but decays to low levels near the outer edge.

These results, which are in accord with those of Kovaszany et al.[11] and Fabris[12] for the boundary layer and cylinder wake respectively, indicate that the observed, well-known decay of unconditioned intensities as the outer edge of a shear layer is approached is due largely to the decrease in the percentage of time the flow is turbulent and that the irrotational fluid is far from quiescent.

The corresponding results for the intensity of the fluctuations of helium concentration are shown in Figure 10b. On the centerline we find a relative intensity of 0.23; there are several sets of data for the relative intensity of temperature fluctuations on the centerline of the wake of a cylinder; again there is a range of experimental values. LaRue and Libby[14] give 0.28, Freymuth and Uberoi[15] 0.20, and from Fabris[12] we deduce 0.25. Thus our value is well within the range of previous results.

The zone averaged intensity of the concentration fluctuations actually increases across the jet and appears to approach a value

30% higher than at the centerline. This is in agreement with the results for temperature fluctuations as given by LaRue and Libby[14] but is less than the increase indicated by Fabris[12] whose results in this regard may suffer from insufficient samples for statistical reliability.

These results on the intensity of the fluctuations of the helium concentration indicate that the decay of the unconditioned intensity as the outer edge of the jet is approached is due solely to the decreased percent of time the flow is turbulent and that the fluctuations within the turbulent fluid remains high throughout the jet.

The data on the skewness and kurtosis complete the picture of the statistical behavior of the velocity and concentration but are of less interest. Comparison of the distributions of the two quantities suggests that they are dominated by the variation of the intensities. Also the distributions of skewness and kurtosis indicate that nowhere in the jet is a Gaussian distribution a reasonable approximation.

In concluding this discussion of the unconditioned and zone statistics we remark that some of the results are comparable to those in the far-field of the wake of a cylinder and thus correspond to apparent similarity, despite the earlier indication in terms of gross jet behavior that our measurements do not correspond to the far-field.

Range conditioned point statistics

A picture of the structure of the turbulent zones of various durations can be established by employing a conditioning technique which we term range conditioned point statistics.[14] This technique was developed independently by Antonia.[16] To understand the technique consider a point within the jet where the flow is intermittent to a significant extent, e.g., where $\gamma = 0.5$. The time intervals for turbulent fluid to pass the point in question have a complete distribution from short times corresponding either to small turbulent structures or to grazes off the centerplane of larger structures and to long times corresponding to passages through the center of large structures. We can select a subset of these passages that are within a small, specified tolerance of a nominal duration, can divide the passage time into equal time intervals from the upstream and downstream crossings, and can carry out statistical analysis of the velocity and helium concentration at these times. The result is termed range conditioned point statistics and provides a statistical picture of turbulent structures of a given size provided the time durations are converted to spatial dimensions by application of Taylor's hypothesis. The zone averages discussed earlier correspond to averaging over all points within a turbulent structure of a given size and again over all sizes. It can be appreciated that because of the heavy conditioning involved in this technique extended time records are required to achieve statistical reliability. For the present results there are at least 50 samples used for each data point.

We present data corresponding to two points within the jet at a streamwise station corresponding to $\left((x - x_{ou})/\theta\right) = 16.1$; Figures 12 and 13 present the results for the velocity and helium concentration at a lateral position corresponding to $\left(y\left((x - x_{ou})\theta\right)^{-\frac{1}{2}}\right)$ 0.41 where $\gamma = 0.86$, i.e., where the flow is turbulent most of the time. Figures 14 and 15 do likewise for a lateral position corresponding to $\left(y\left((x - x_{ou})\theta\right)^{-\frac{1}{2}}\right) = 0.57$ where $\gamma = 0.34$. Several nominal *durations at each station with a tolerance of 10% are considered.* The durations are presented in terms of multiples of digital time steps; the equal time intervals are measured relative to either the upstream or downstream crossing so that the tolerance accepted for the nominal duration is accommodated in the central region where the various statistical quantities are found to change gradually. The data points located relative to the upstream edge are open symbols, those from the downstream edge are half-shaded.

It should be recalled in the present context that discrimination between turbulent and irrotational fluid is based on a level of helium as discussed earlier and that this discrimination is applied to the velocity as well. Thus we implicitly assume a single interface for momentum and concentration, an assumption which will be seen later to be consistent with the experimental results. Finally, we note that in order to facilitate interpretation of the results the distributions of various statistical quantities have been presented with the upstream edges aligned.

In Figures 12a and 14a we see the distributions of velocity through turbulent zones of four durations; the dashed lines on these figures is the velocity in the external stream. From these data several observations may be made; the velocity at the two interfaces is continuous and increases smoothly across the interface with a steeper gradient at the downstream edges. In the central portion of the zones, i.e., remote from the interfaces, the velocity increases from the upstream to the downstream edges, implying that the stretching of the zones in the streamwise direction is associated with the movement of the downstream edges away from the upstream edges. This also suggests, as we shall confirm later in connection with the results relative to the concentration, that entrainment of the slower moving air occurs primarily on the upstream edges of the zones. Finally, comparison of the distributions at the two lateral positions indicates that the shorter turbulent zones further from the jet centerline have velocities close to U_∞ so that the positive increment of the turbulent zone averages over U_∞ is due to the large turbulent structures.

The distributions of root-mean-square velocity intensities shown in Figures 12b and 14b indicate smooth gradients at the two interfaces and relatively flat regions in the central portions of the zones. The gradients of intensity are greater at the downstream edges, again consistent with greater entrainment of low velocity air at the upstream edges with consequent higher intensities there.

We now turn to the distributions of helium concentration: Figures 13a and 15a display the distributions of mean helium concentration through turbulent zones of various durations. Three reasonably distinct regions in each zone can be identified; there are two interfacial regions involving relatively steep gradients of concentration. The structure of the upstream interfaces are essentially the same independent of duration but those associated with the longer zones involve greater increases in concentration before fairing into the third, central region. The extent of this third region depends on the duration of the zone, but independent of duration, displays a gradual increase in helium concentration from the upstream to the downstream interfacial regions.

For zones of longest duration it appears that the mean concentration approaches a constant. We shall see subsequently that the skewness of the concentration fluctuations for these zones of long duration suggests a well-stirred mixture without the obvious presence of newly entrained air. Finally, comparison of these two figures indicates little difference in the distributions of mean concentration with the two values of γ considered.

We conclude from these data that entrainment of air from the external flow occurs to a greater extent on the upstream edges of the turbulent zones. This supports the observations made earlier on the basis of the range conditioned point statistics of the velocity. Of special interest is to compare these results with the temperature measurements of LaRue and Libby[14] which imply preferential entrainment on the downstream edges of the turbulent zones. The difference is attributable to the difference in the velocity of the turbulent zones relative to the external flow; in the case of the wake the turbulent fluid moves slower than the external stream and entrainment on the leeward, i.e., downstream, *surfaces of the turbulent* zones dominates. In the two-dimensional jet considered here the turbulent fluid moves faster than the external stream and again entrainment on the leeward edges dominates. We note that there is no theoretical explanation for these results which would appear to be of fundamental interest.

We note that these observations concerning greater entrainment at the upstream interfacial regions do not establish whether the entrainment mechanism is associated with engulfment or molecular processes. We would deduce on the basis of measurements of the statistical geometry of the interface in the turbulent heated wake by Paizis and Schwartz[17] and LaRue and Libby[18] that in our jet flow the number of overhangs suggestive of engulfment is greater on the leeward, i.e., upstream, edges of the turbulent zones, but whether this coincidence accounts for the observed preferential entrainment is uncertain.

The distributions of the intensities of the concentration fluctuations are shown in Figures 13b and 15b. They support our earlier conclusions concerning entrainment and show smooth increases in intensities in the two interfacial regions and gradual increases from the upstream to the downstream edges.

Although the statistical reliability may be marginal, we show in Figure 13c the distributions of the skewness of the concentration fluctuations for the position closest to the jet centerline. Of interest is the large skewness in the two interfacial regions and the small skewness in the central portions of each turbulent zone. The implications from these data are that the central regions involve nearly symmetrically distributed values of the concentration whereas the freshly entrained fluid involves highly skewed distributions. These results are in agreement with those for temperature given by LaRue and Libby.[14]

An examination of the interface regions given by these data exposes several points of interest. Consider the downstream interfaces as given, e.g., by the intensity of the velocity fluctuations in Figure 12b and by the mean helium concentration in Figure 13a. We find that the thickness of the two interface regions is essentially the same despite the low value for the Schmidt number for dilute helium in helium-air mixtures, namely 0.24. It might be expected that this low value would lead to a significantly thicker interface for helium than for velocity. We thus appear to have evidence in support of the commonly employed assumption, frequently implicit, that the velocity and scalar interface between the turbulent and irrotational fluid are coincident.*

We can use the range conditioned point statistics of the mean concentration to estimate the thicknesses of the interfacial regions. We select the downstream edges for examination since they are somewhat cleaner. We estimate from application of Taylor's hypothesis that the downstream interface is typically 9 mm thick. This can be compared with the Kolmogoroff and Batchelor lengths as follows: From the spectrum of the velocity in the fully turbulent region of the jet we estimate the Kolmogoroff length ℓ_k to be 0.14 mm. The Batchelor length is $\ell_k(Sc)^{-\frac{1}{2}}$ or 0.29 mm. Thus a typical interface is found to be 55 times the Batchelor length. This is considerably thicker than the estimate of $8\ell_k$ obtained by LaRue and Libby[14] for the thickness of the temperature interface in the heated wake.

---

*We intend to repeat the present experiment with the helium heated; in this case it will be of interest to compare the concentration and temperature interfaces and to establish whether the differences in Schmidt and Prandtl numbers will result in distinguishable interface thicknesses.

The reason for this increase in relative thickness is unknown; it may be due to the reduction in the Schmidt number relative to the Prandtl number but it might be expected that this should be accounted for by the comparison of the interface thickness with the Batchelor scale rather than the Kolmogoroff scale.

IV. CONCLUSIONS

We find the downstream development of the turbulent helium jet to be in reasonable agreement with earlier experiments of plane jets in moving streams. Although strict similarity does not apply in this region of jet flow, turbulent zone statistics of concentration for the mean and relative intensity distributions resemble turbulent zone statistics of temperature in the wake of a heated cylinder.

The conditioned velocity statistics show that the non-turbulent fluid well within the jet is moving faster than the free stream velocity.

Distributions through turbulent zones of various durations obtained by ranged conditioned point statistics show that entrainment at the upstream interfacial regions is dominant, that the concentration and momentum interfaces cannot be distinguished, and finally that the concentration interface is considerably thicker than that inferred from measurements of temperature in the wake of a heated cylinder. The findings relative to entrainment are consistent with previous results in that entrainment at the leeward interface of the turbulent zone dominates.

REFERENCES

1. Rodi, W., A Review of Experimental Data of Uniform Density Free Turbulent Boundary Layers, in Studies in Convection Vol. 1, edited by Brian Launder (Academic Press, London, 1975).

2. Weinstein, A. S., Osterle, J. F. and Forstall, W., Momentum Diffusion from a Slot Jet into a Moving Secondary, J. Appl. Mech., 23, 437-443 (1956).

3. Bradbury, L. J. S. and Riley, J., The Spread of a Turbulent Plane Jet Issuing into a Parallel Moving Airstream, J. Fluid Mech., 27, 381-394 (1967).

4. Everitt, K., Ph.D. thesis, University of London (1971).

5. Kotsovinos, Nikolas E., A Note on the Spreading Rate and Virtual Origin of a Plane Turbulent Jet, J. Fluid Mech., 77, 303-311 (1977).

6. Way, J. and Libby, P. A., Application of Hot-wire Anemometry and Digital Techniques to Measurements in a Turbulent Helium Jet, AIAA J., 9, 1567-1573 (1971).

7. LaRue, J. C. and Libby, P. A., Measurements in the Turbulent Boundary Layer with Slot Injection of Helium, Phys. of Fluids, 20, 192-202 (1977).

8. Stanford, R. A. and Libby, P. A., Further Applications of Hot-wire Anemometry to Turbulence Measurements in Helium-Air Mixtures, Phys. of Fluids, 17, 1353-1361 (1974).

9. Schlicting, H., Boundary Layer Theory (McGraw Hill, New York, 1955), pp. 492-494.

10. Libby, P. A., Prediction of the Intermittent Turbulent Wake of a Heated Cylinder, Phys. of Fluids, 19, 494-501 (1976).

11. Kovasznay, L. S. G., Kibens, V. and Blackwelder, R. F., Large-scale Motion in the Intermittent Region of a Turbulent Boundary Layer, J. Fluid Mech., 41, 283-325 (1970).

12. Fabris, G., Ph.D. thesis, Illinois Institute of Technology, 1974. See also: Turbulent Temperature and Thermal Flux Characteristics in the Wake of a Cylinder. Symposium on Turbulent Shear Flows, April 18-20, 1977, University Park, Pennsylvania, pp. 1511-20.

13. Townsend, A. A., The Structure of Turbulent Shear Flows (Cambridge University Press, 1956), pp. 131-168.

14. LaRue, J. C. and Libby, P. A., Temperature Fluctuations in the Plane Turbulent Wake, Phys. of Fluids, 17, 1956-1967 (1974).

15. Freymuth, P. and Uberoi, M. S., Structure of Temperature Fluctuations in the Turbulent Wake of a Heated Cylinder, Phys. of Fluids, 14, 2574-2580 (1971).

16. Antonia, R. A., Conditionally Sampled Measurements near the Outer Edge of a Turbulent Boundary Layer, J. of Fluid Mech., 56, 1-18 (1972).

17. Paizis, S. T. and Schwarz, W. H., An Investigation of the Topography and Motion of the Turbulent Interface, J. Fluid Mech., 63, 315-343 (1974).

18. LaRue, J. C. and Libby, P. A., Statistical Properties of the Interface in the Turbulent Wake of a Heated Cylinder, Phys. of Fluids, 19, 1864-1875 (1976).

LIST OF FIGURES

8. Distribution of crossing frequency (See Figure 7 for symbol identification)

9. Unconditioned and turbulent zone statistics for the velocity (See Figure 7 for symbol identification. Flagged symbols indicate turbulent zone values and refer to scale on right.)

   a. Mean values

   b. Root-mean-square intensity

   c. Skewness φ

   d. Kurtosis

10. Unconditioned and turbulent zone statistics for the concentration of helium (See Figures 7 and 9 for symbol identification)

    a. Mean values

    b. Root-mean-square intensity

    c. Skewness

    d. Kurtosis

11. Irrotational zone statistics of the velocity (See Figures 7 and 9 for symbol identification)

    a. Mean values

    b. Root-mean-square intensity

    c. Skewness

    d. Kurtosis

12. Range conditioned point statistics for the velocity: $\gamma = 0.846$

   a. Mean values

   b. Root-mean-square intensity

13. Range conditioned point statistics for the concentration of helium: $\gamma = 0.84$

   a. Mean values

   b. Root-mean-square intensity

   c. Skewness

14. Range conditioned point statistics for the velocity: $\gamma = 0.34$

   a. Mean values

   b. Root-mean-square intensities

15. Range conditioned point statistics for the concentration of helium: $\gamma = 0.34$

   a. Mean values

   b. Root-mean-square intensities

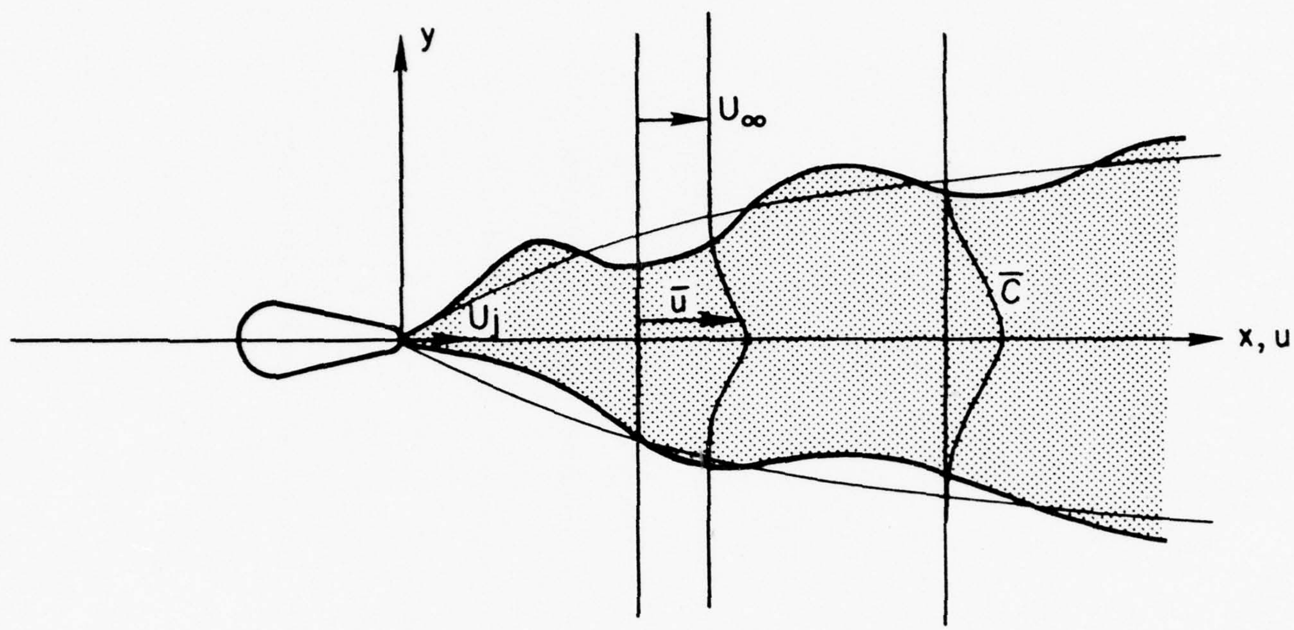

Figure 1. Schematic representation of the flow

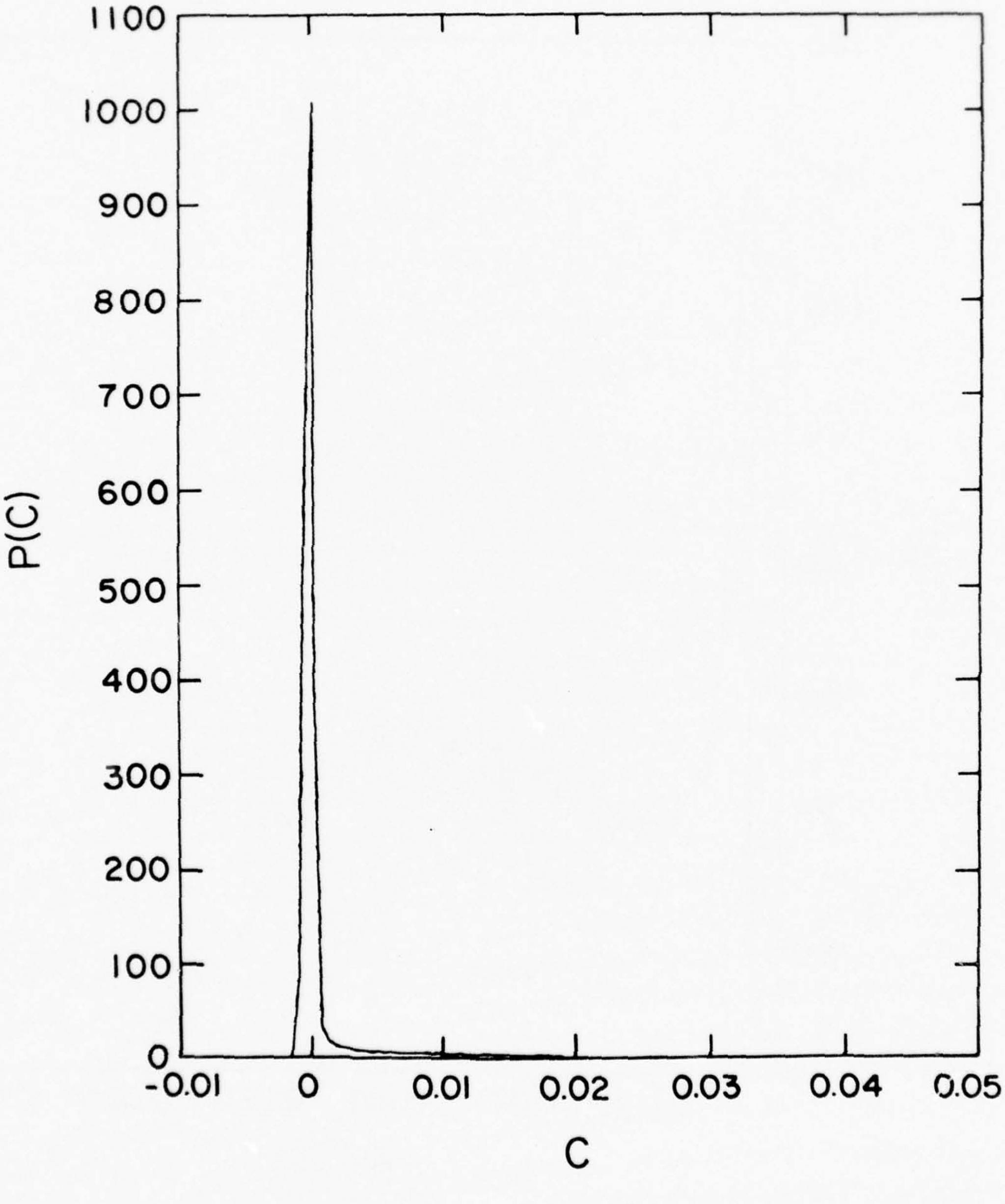

Figure 2. Probability density functions of concentration

a. = 0.14

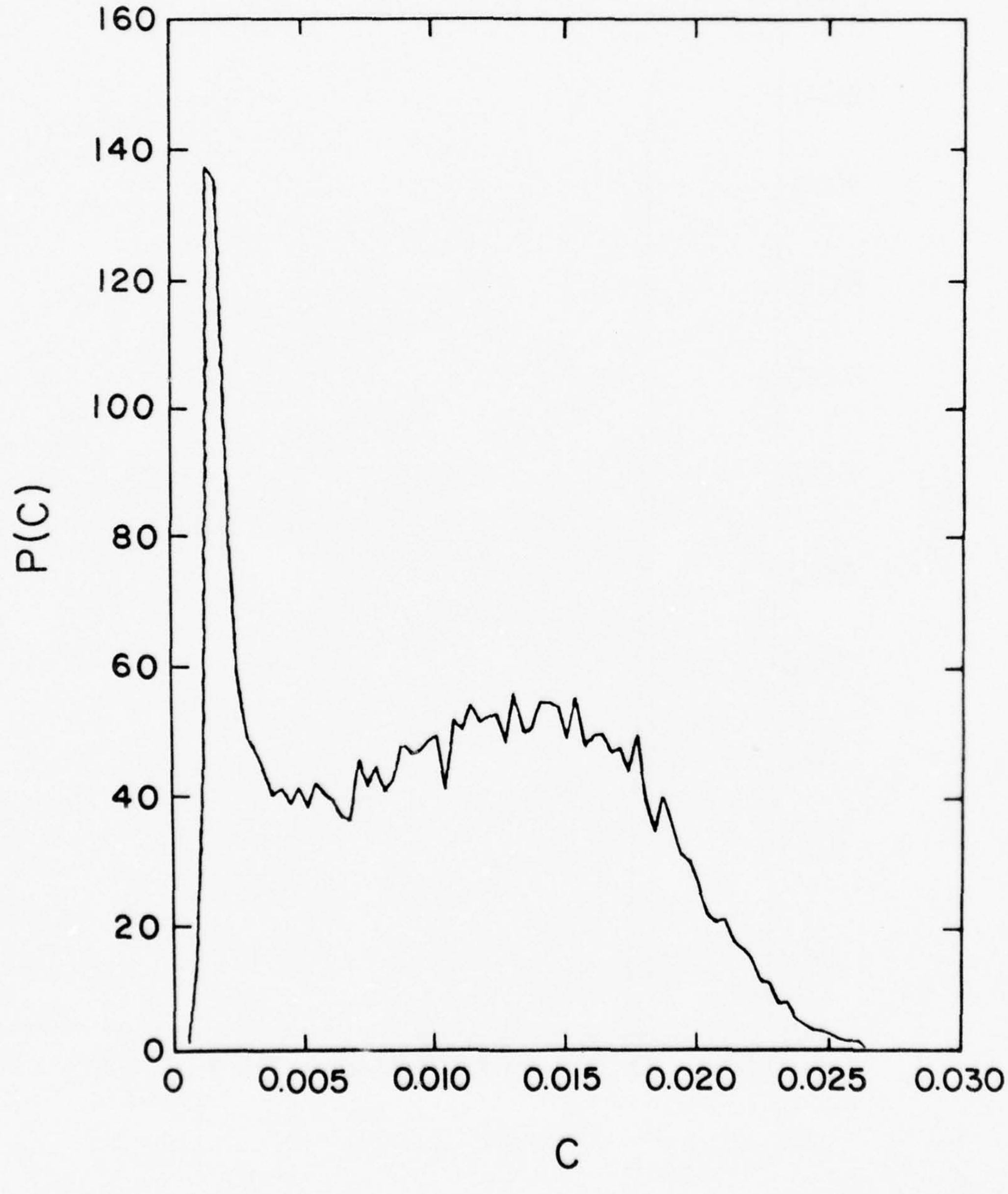

Figure 2b.   = 0.84

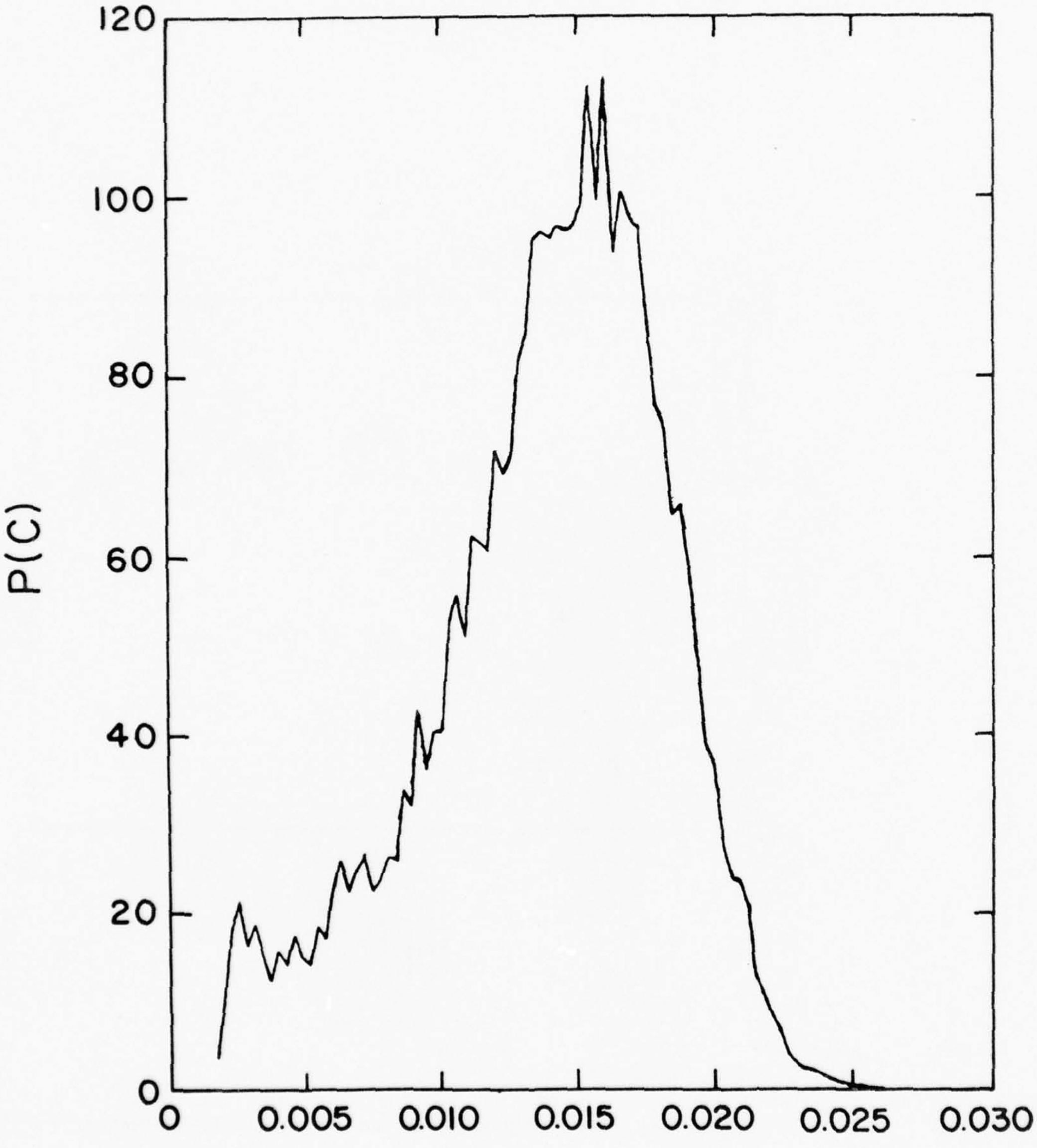

Figure 2c. = 0.97

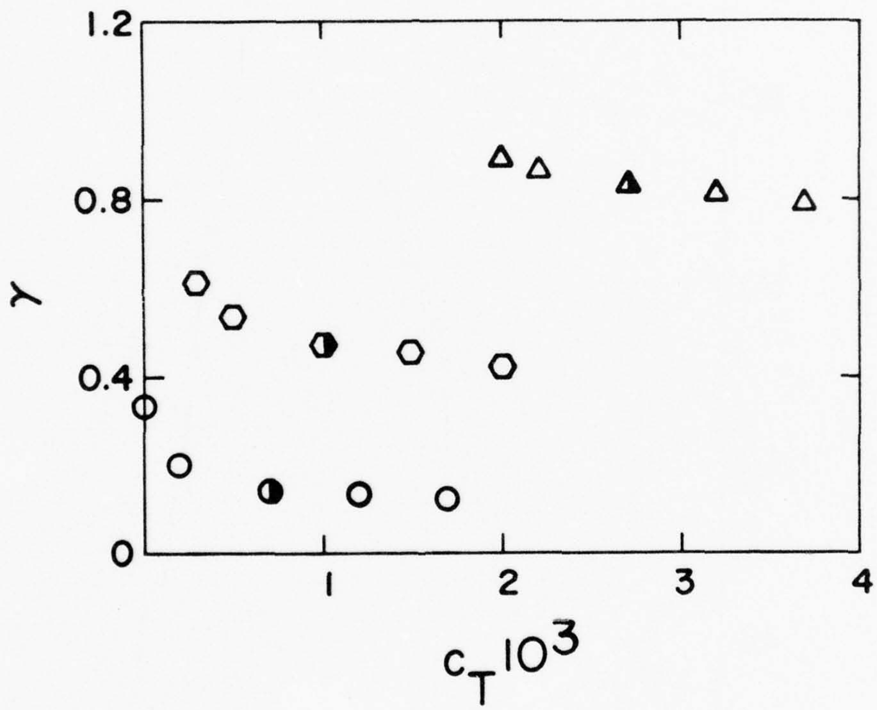

Figure 3. Dependence on the threshold value of concentration x, cm: O : 43; Δ : 131; ⬡ : 174. Half-shaded symbol indicates threshold values selected.

a. Intermittency

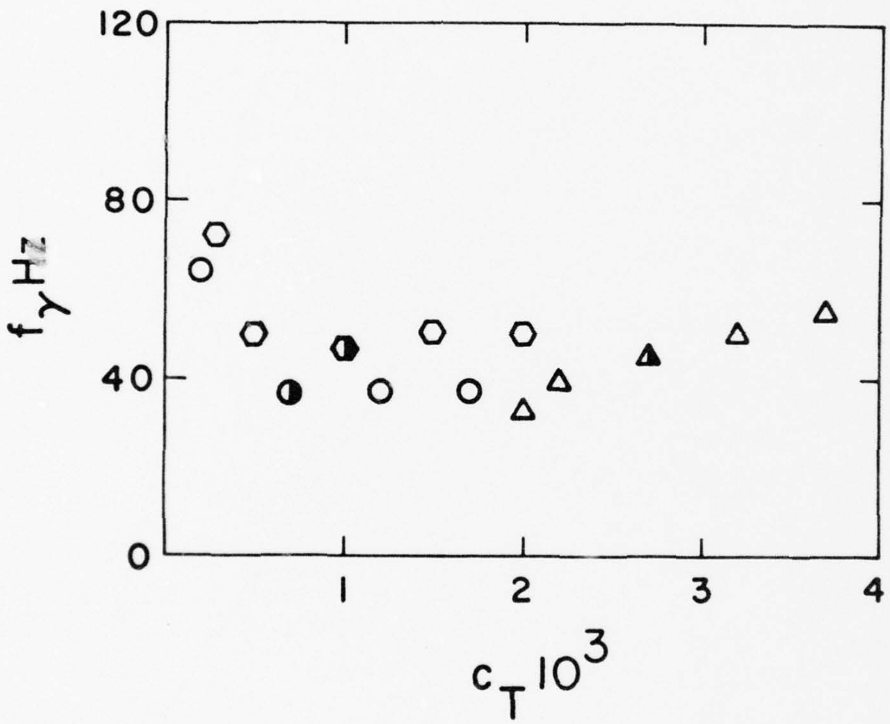

Figure 3b. Crossing frequency

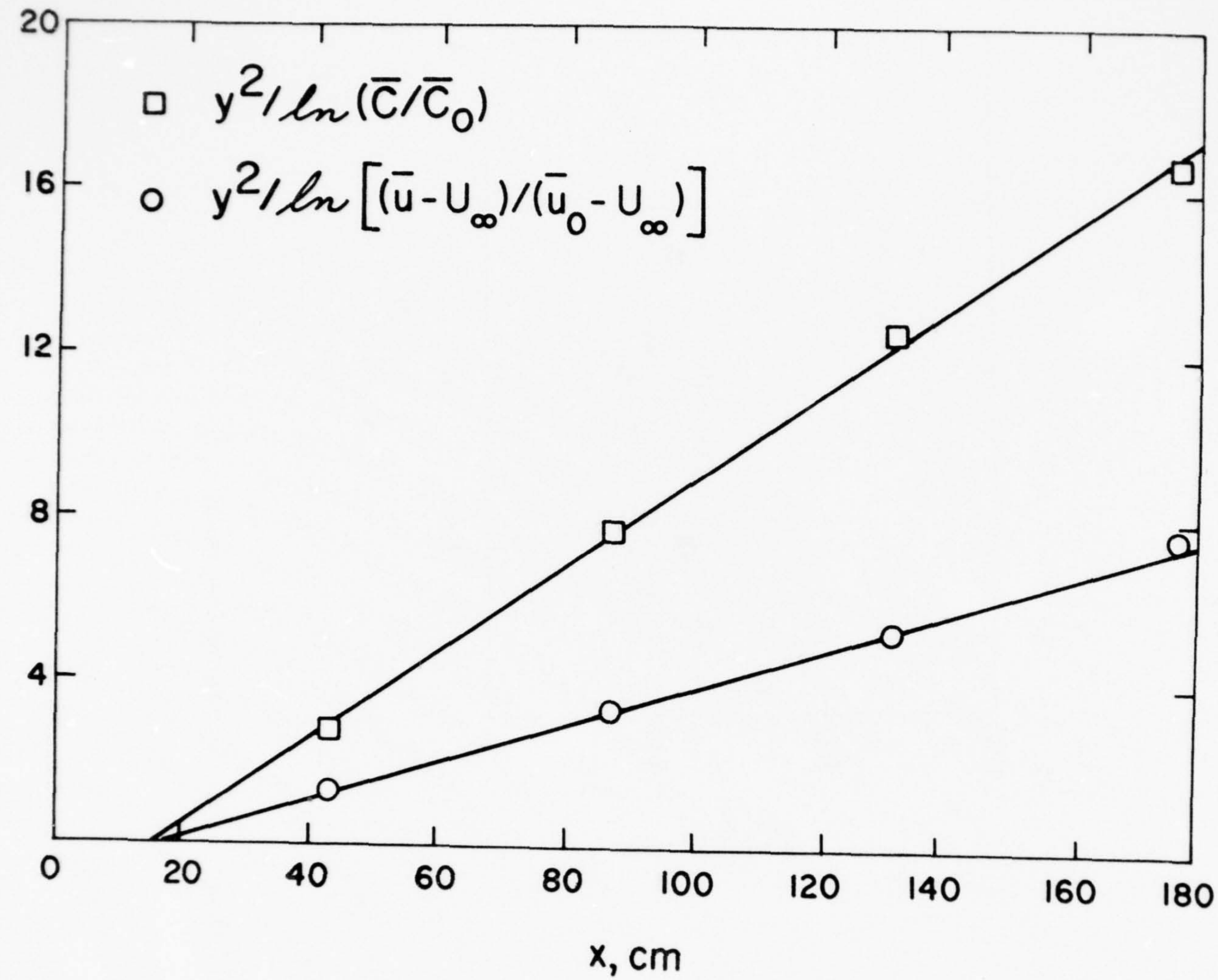

Figure 4. Determination of the apparent virtual origins

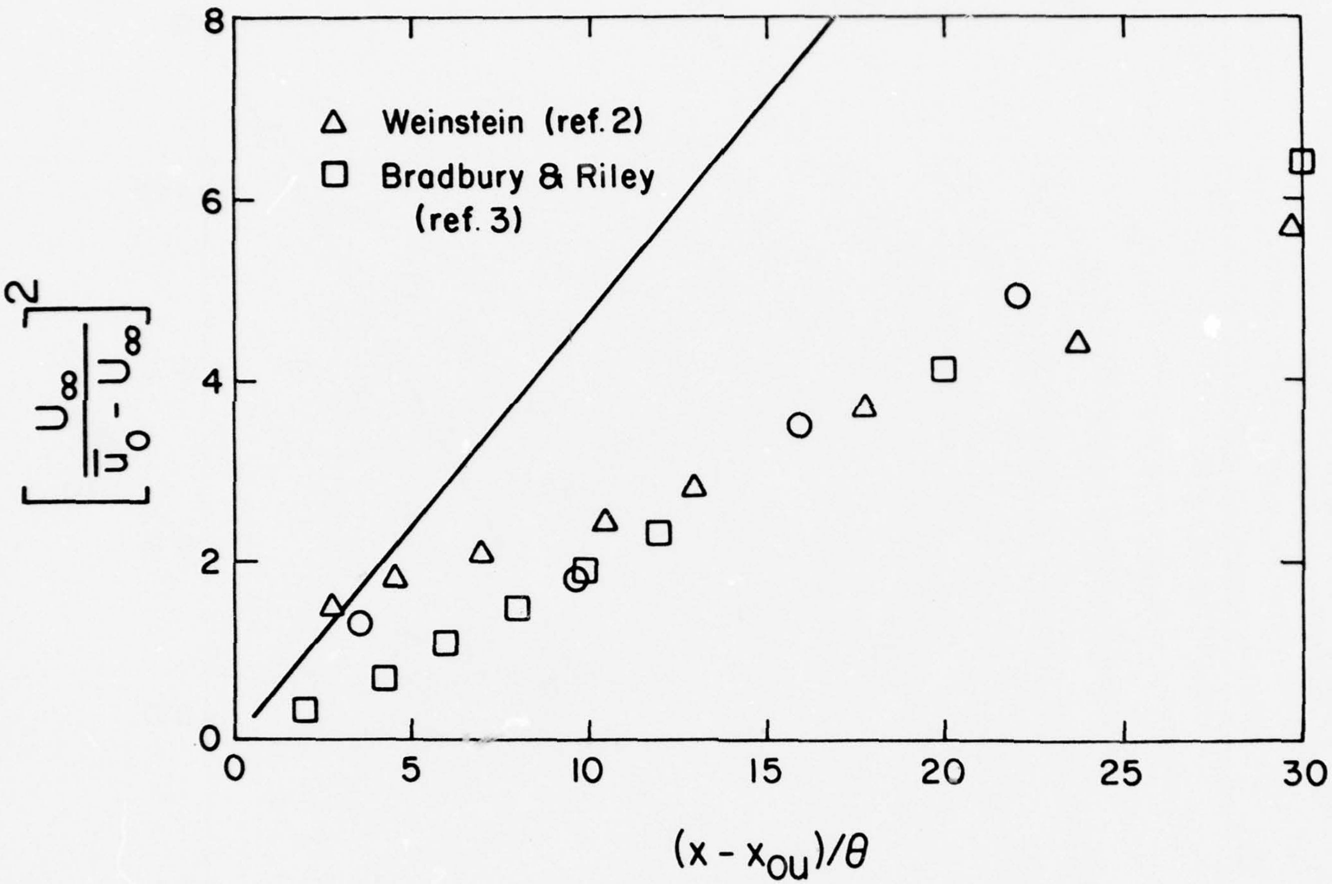

Figure 5. Comparison of gross jet behavior

a. Decay of centerline velocity excess

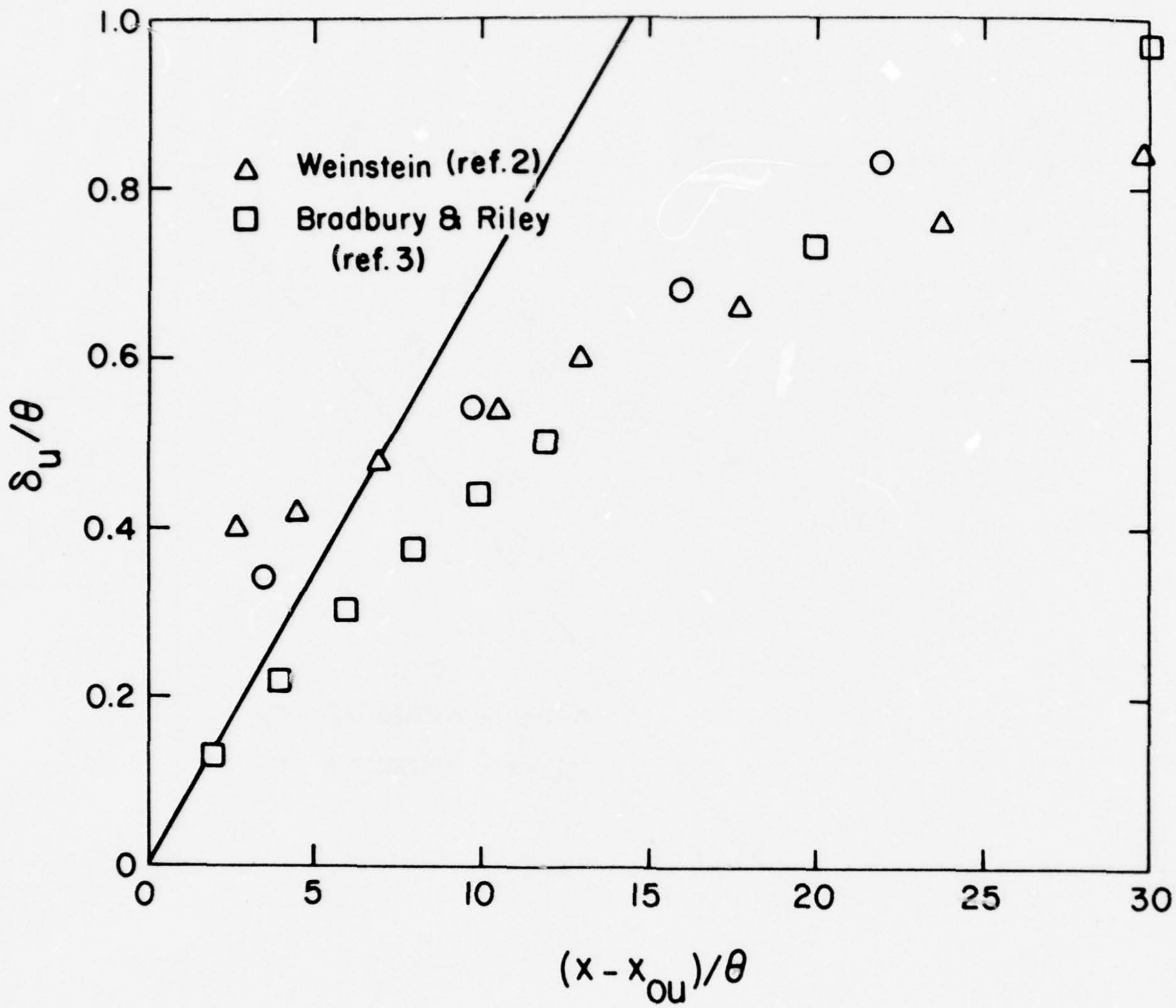

Figure 5b. Growth of half-width of the jet

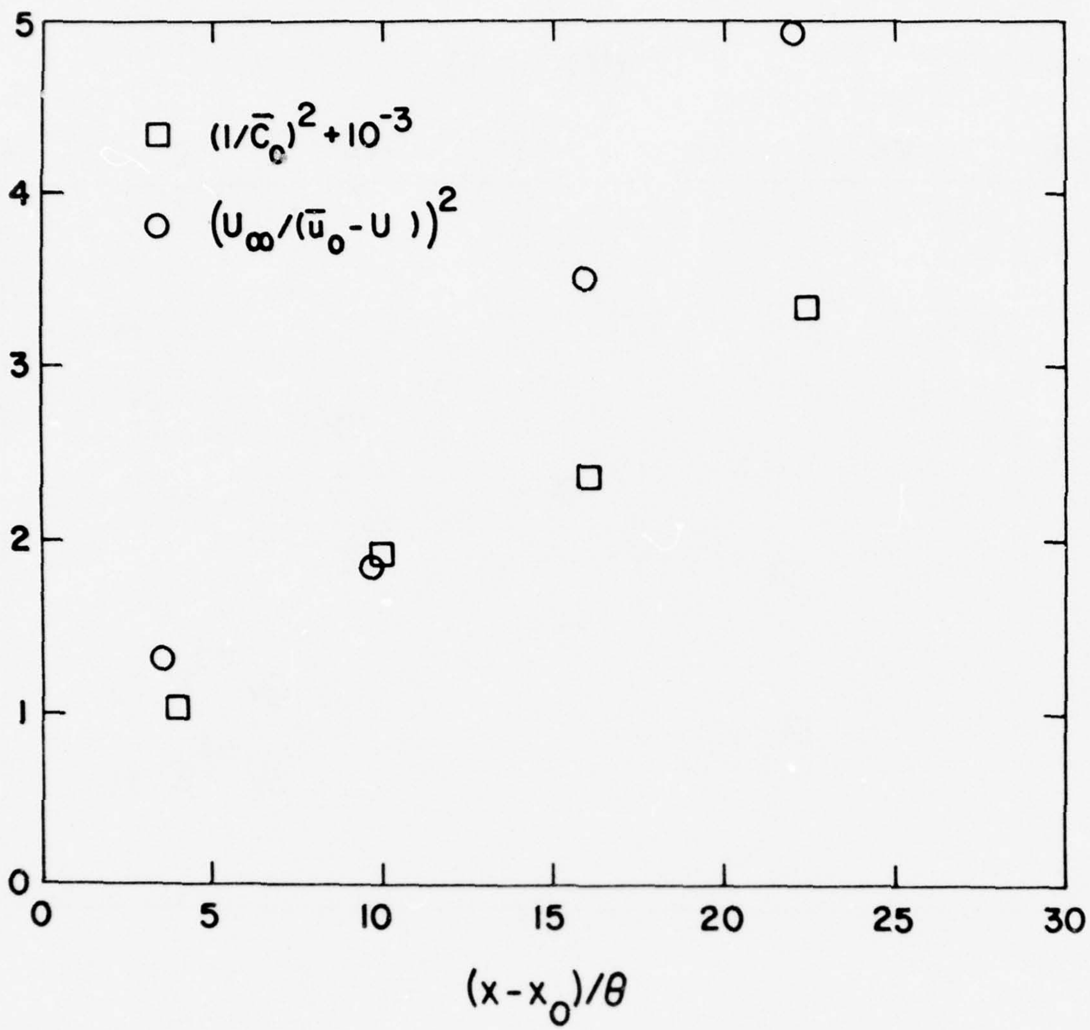

Figure 6. Comparison of the gross behavior of velocity and concentration

a. Decay of centerline velocity and concentration

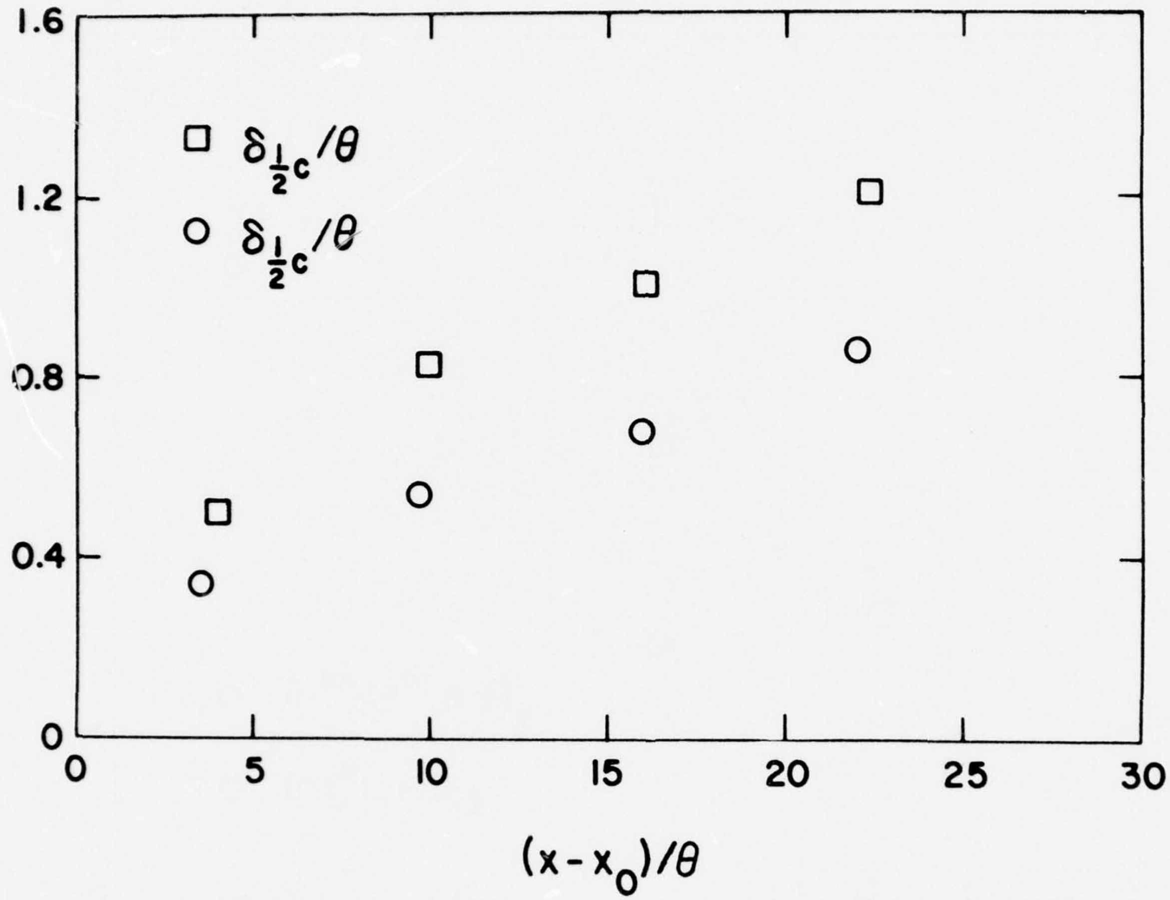

Figure 6b. Growth of half-widths for velocity and concentration

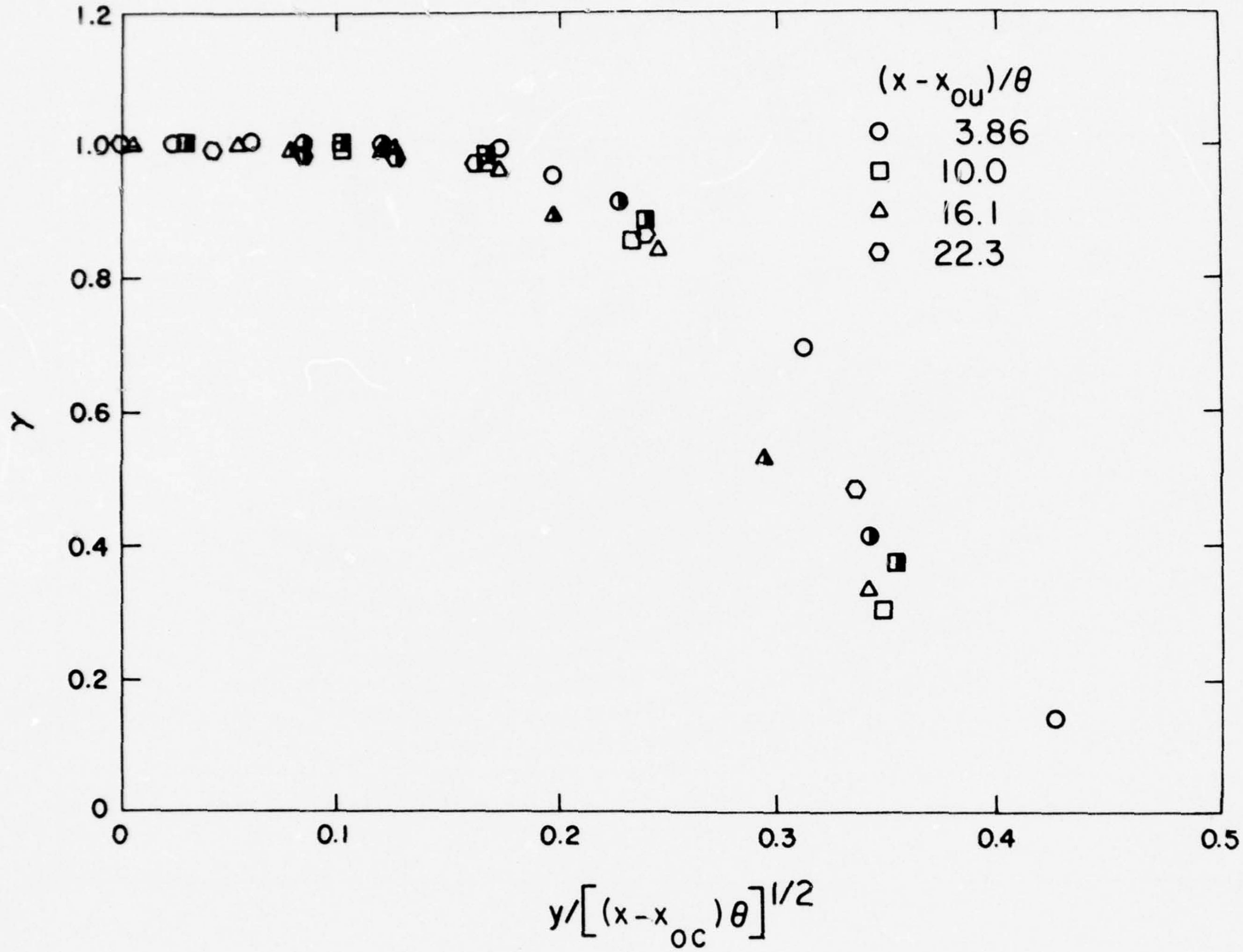

Figure 7. Distribution of intermittency (Half-darkened symbols are from lower half of the jet)

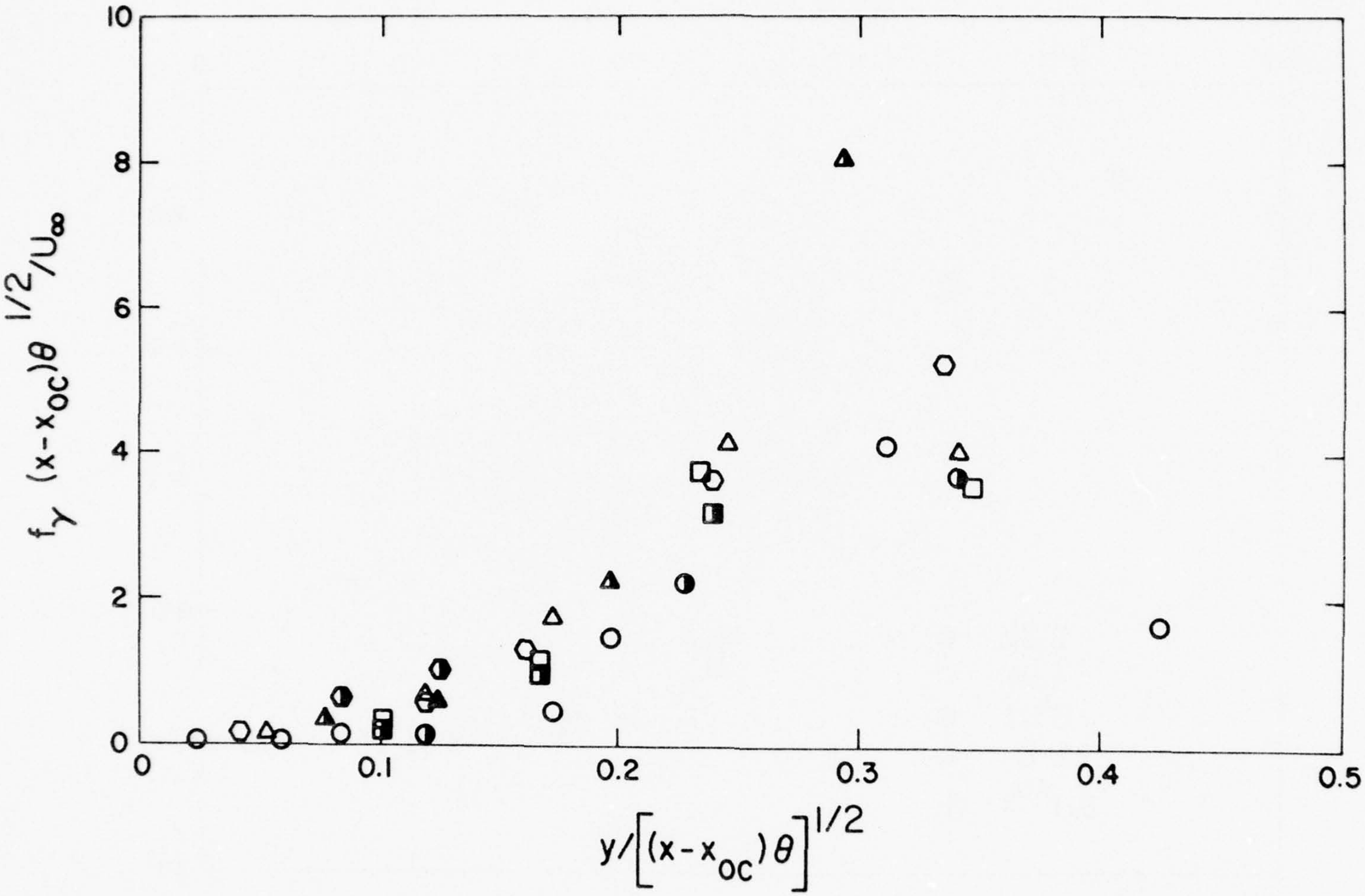

Figure 8. Distribution of crossing frequency (See Figure 7 for symbol identification)

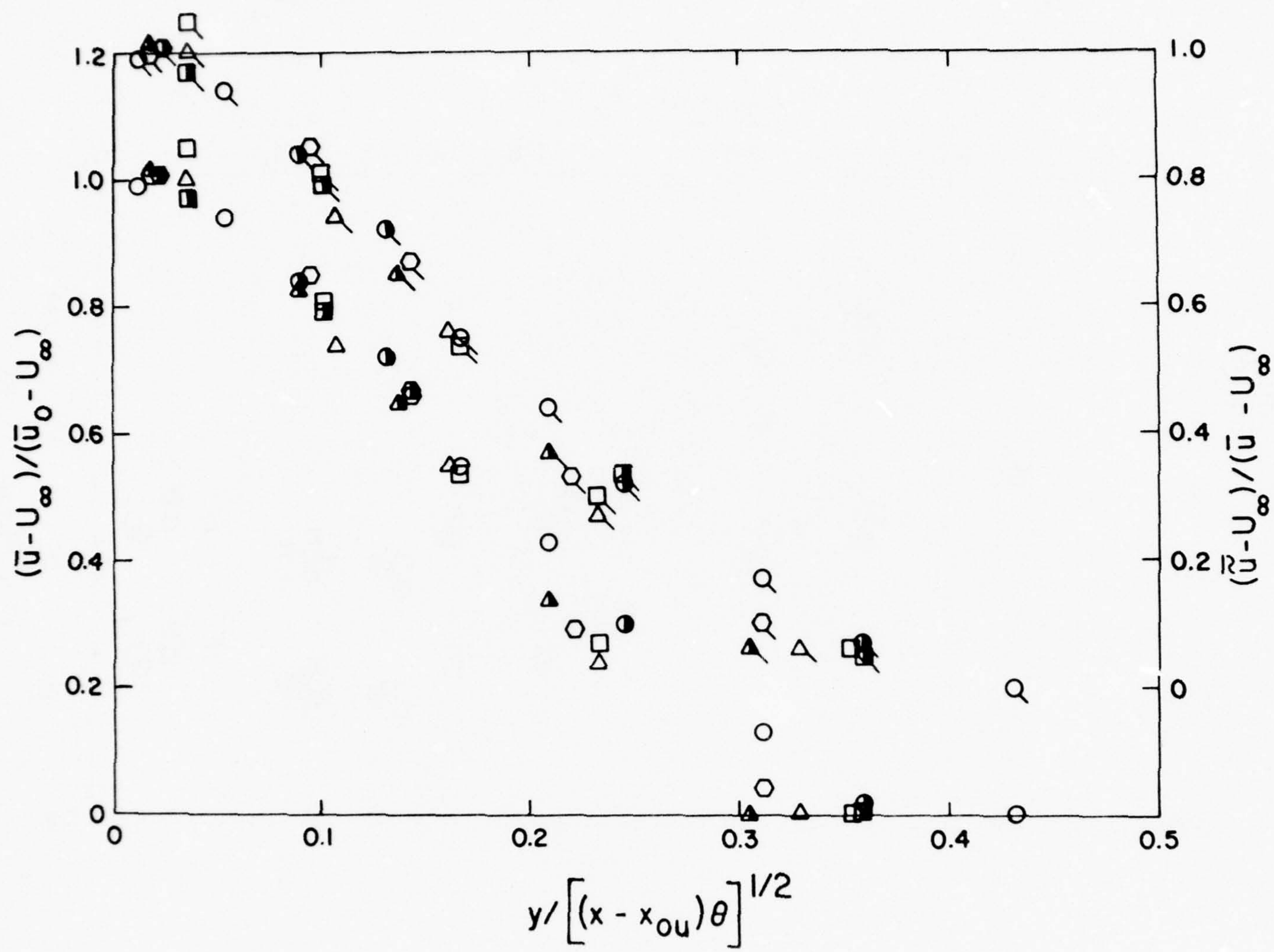

Figure 9. Unconditioned and turbulent zone statistics for the velocity (See Figure 7 for symbol identification. Flagged symbols indicate turbulent zone values and refer to scale on right.) a. Mean values

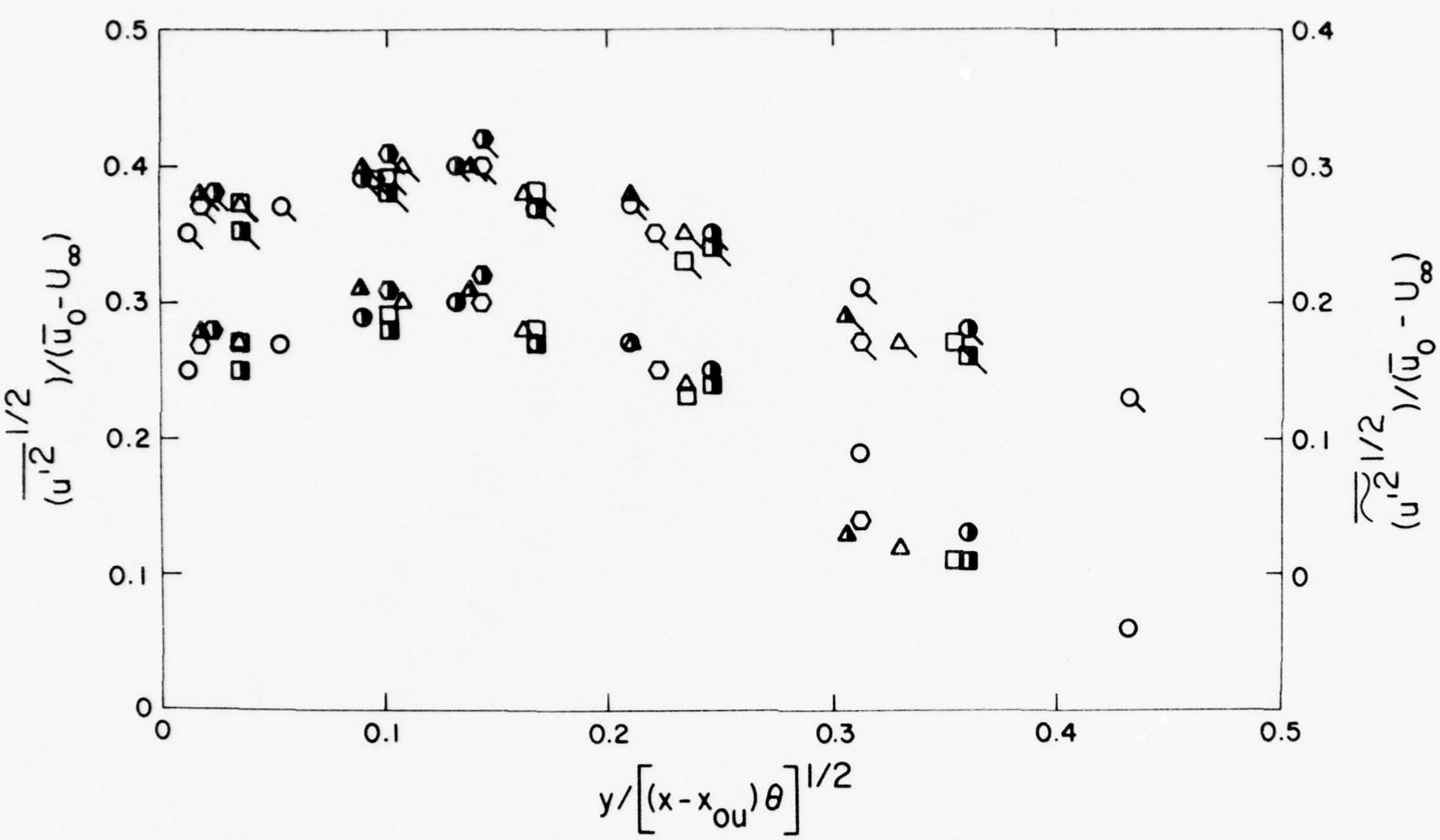

Figure 9b. Root-mean-square intensity

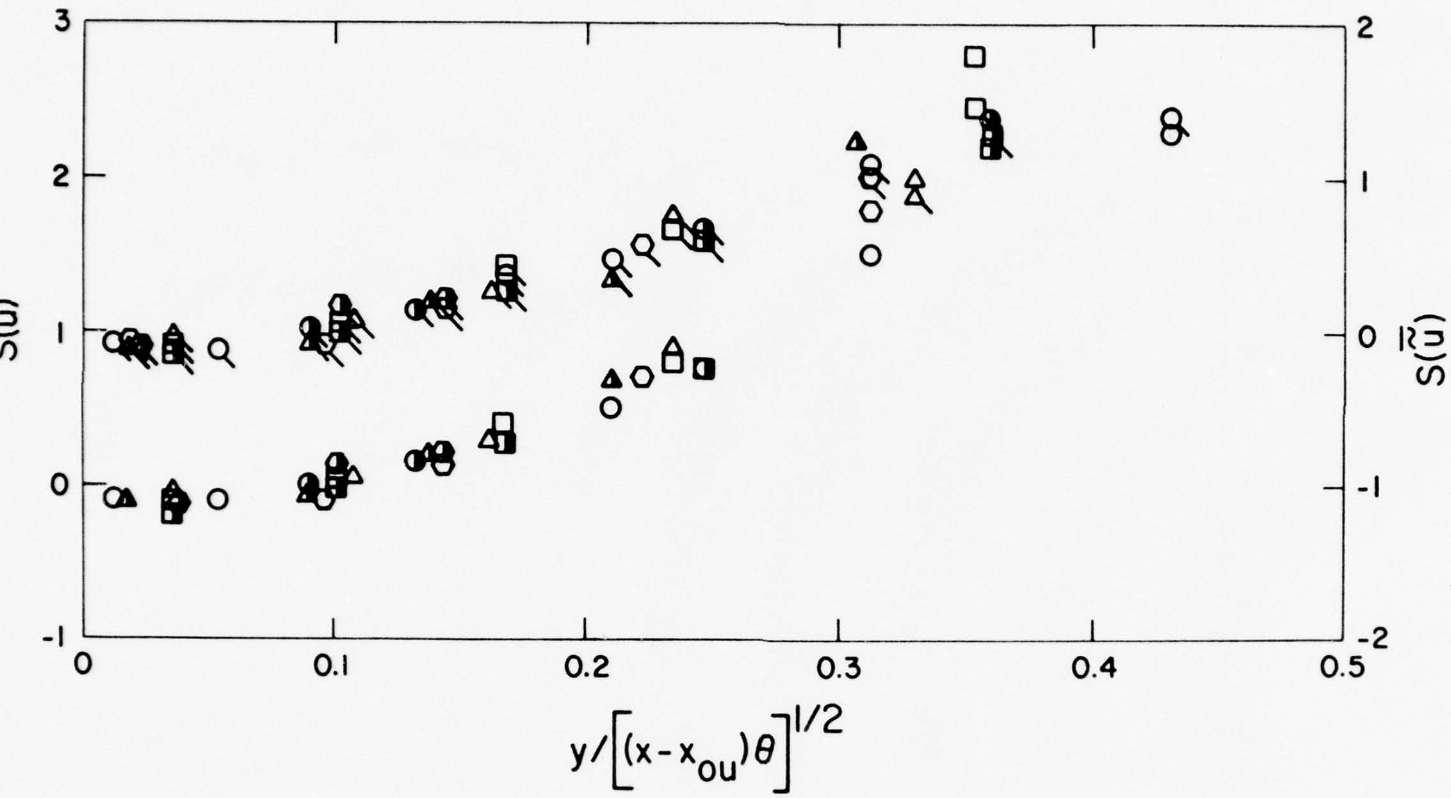

Figure 9c. Skewness φ

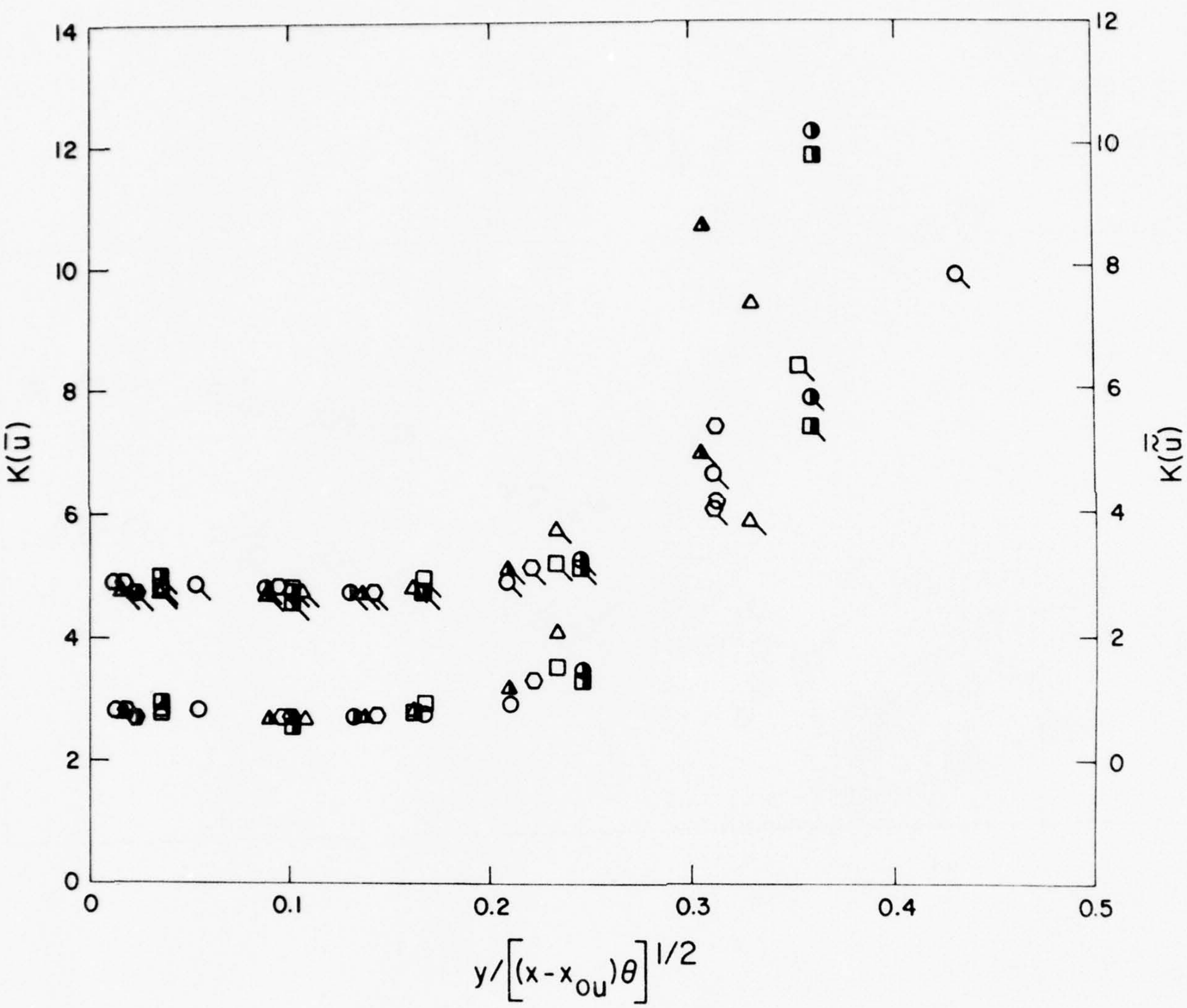

Figure 9d. Kurtosis

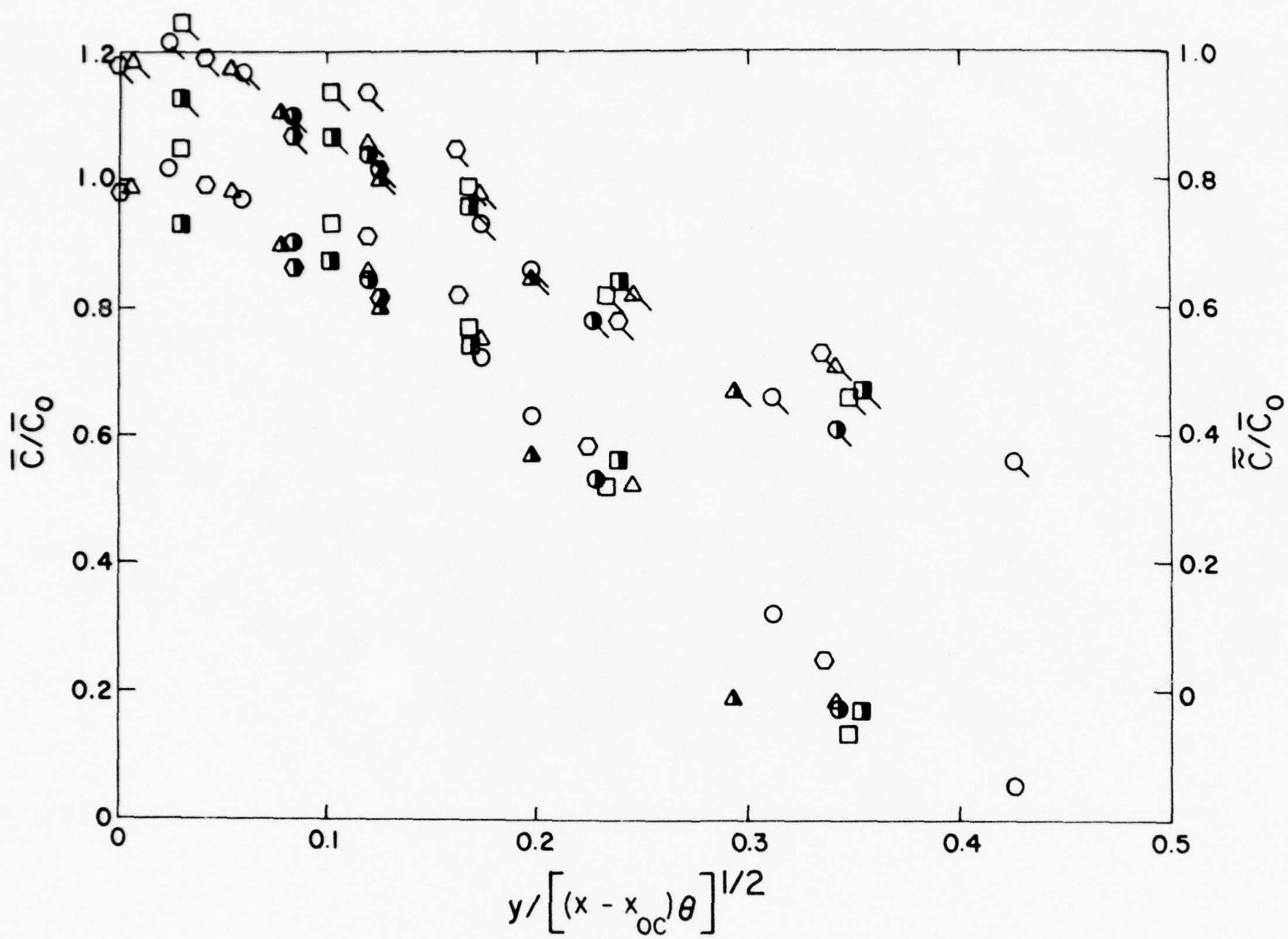

Figure 10. Unconditioned and turbulent zone statistics for the concentration of helium (See Figures 7 and 9 for symbol identification)
a. Mean values

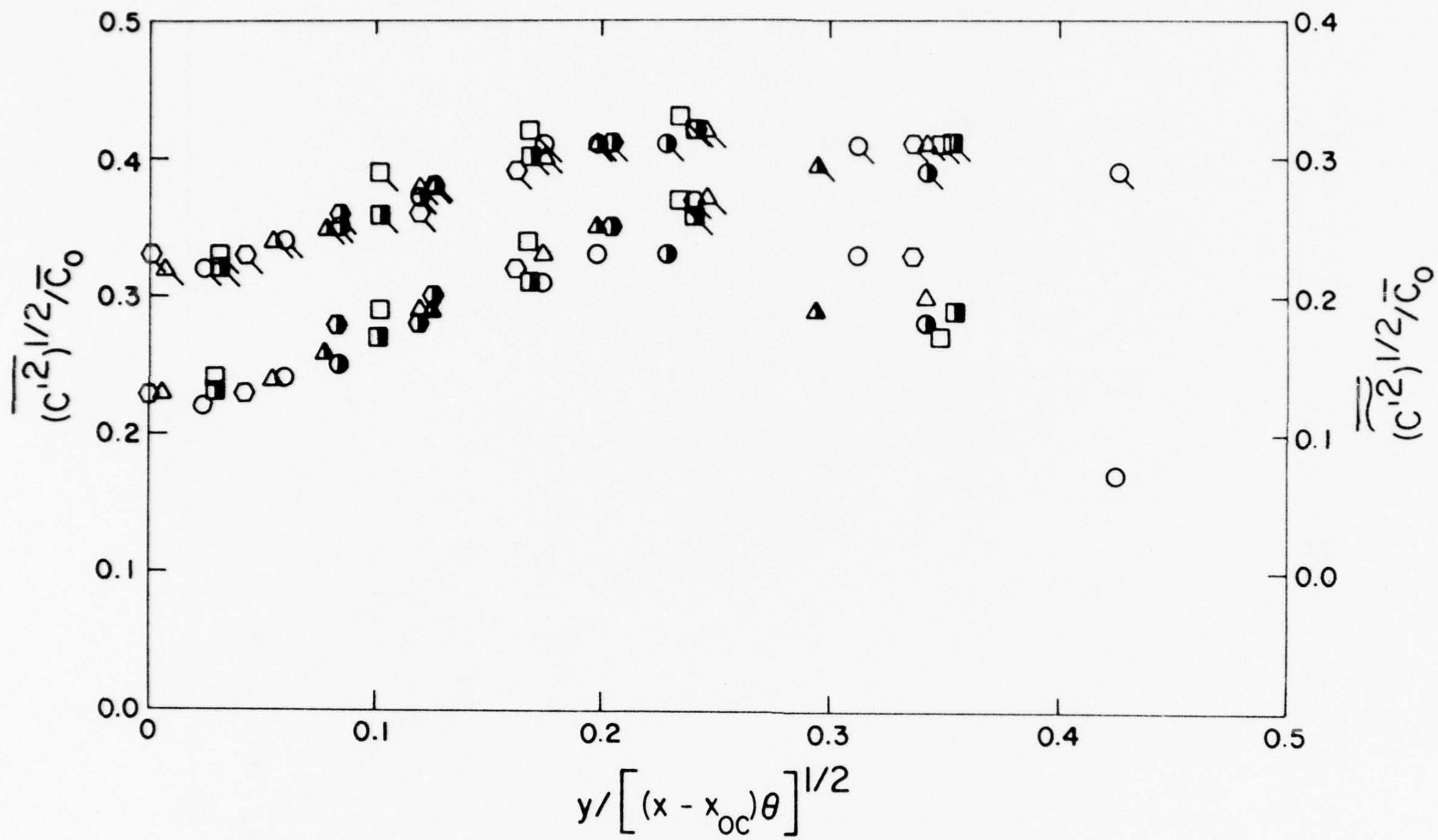

Figure 10b. Root-mean-square intensity

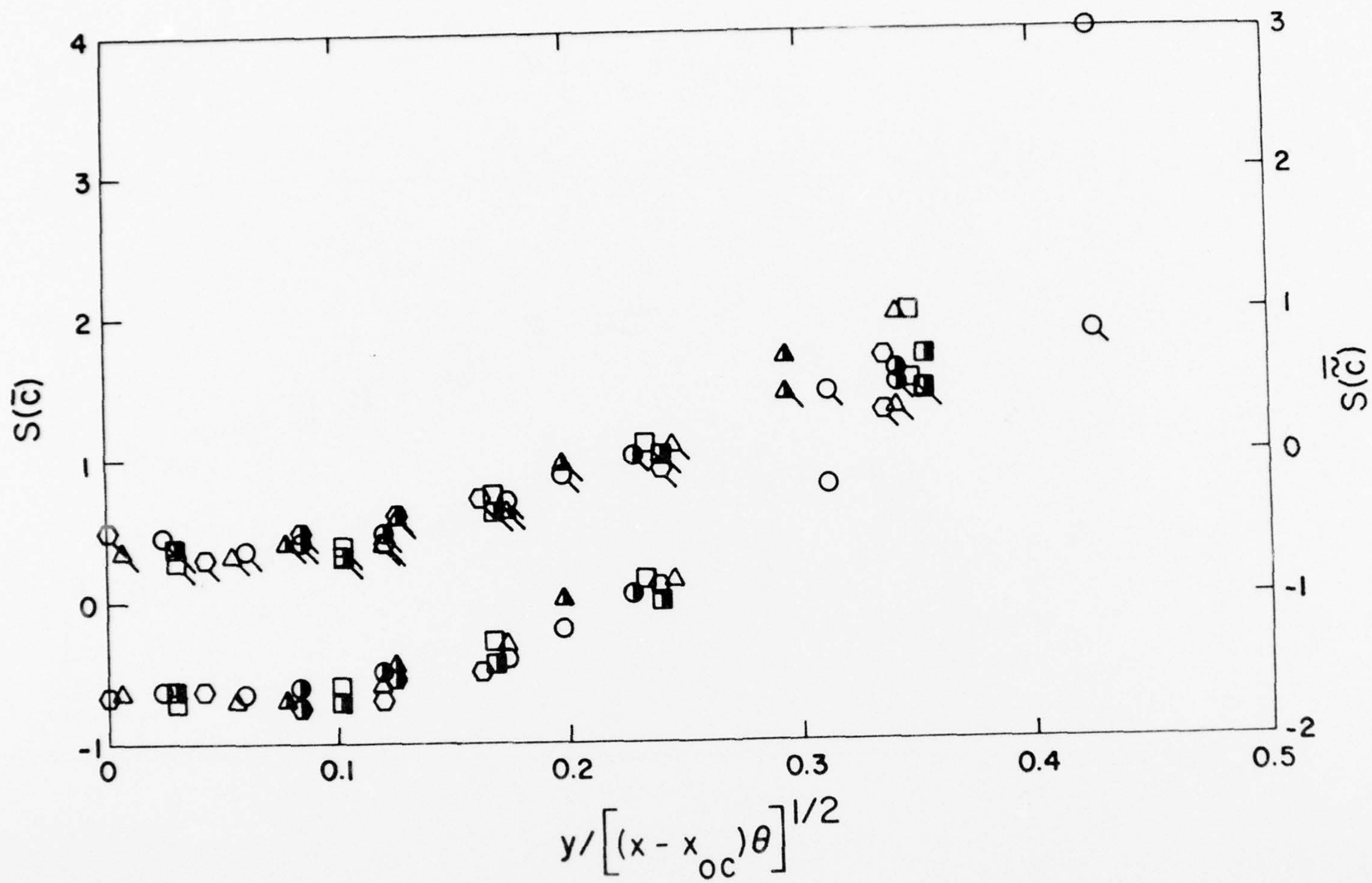

Figure 10c. Skewness

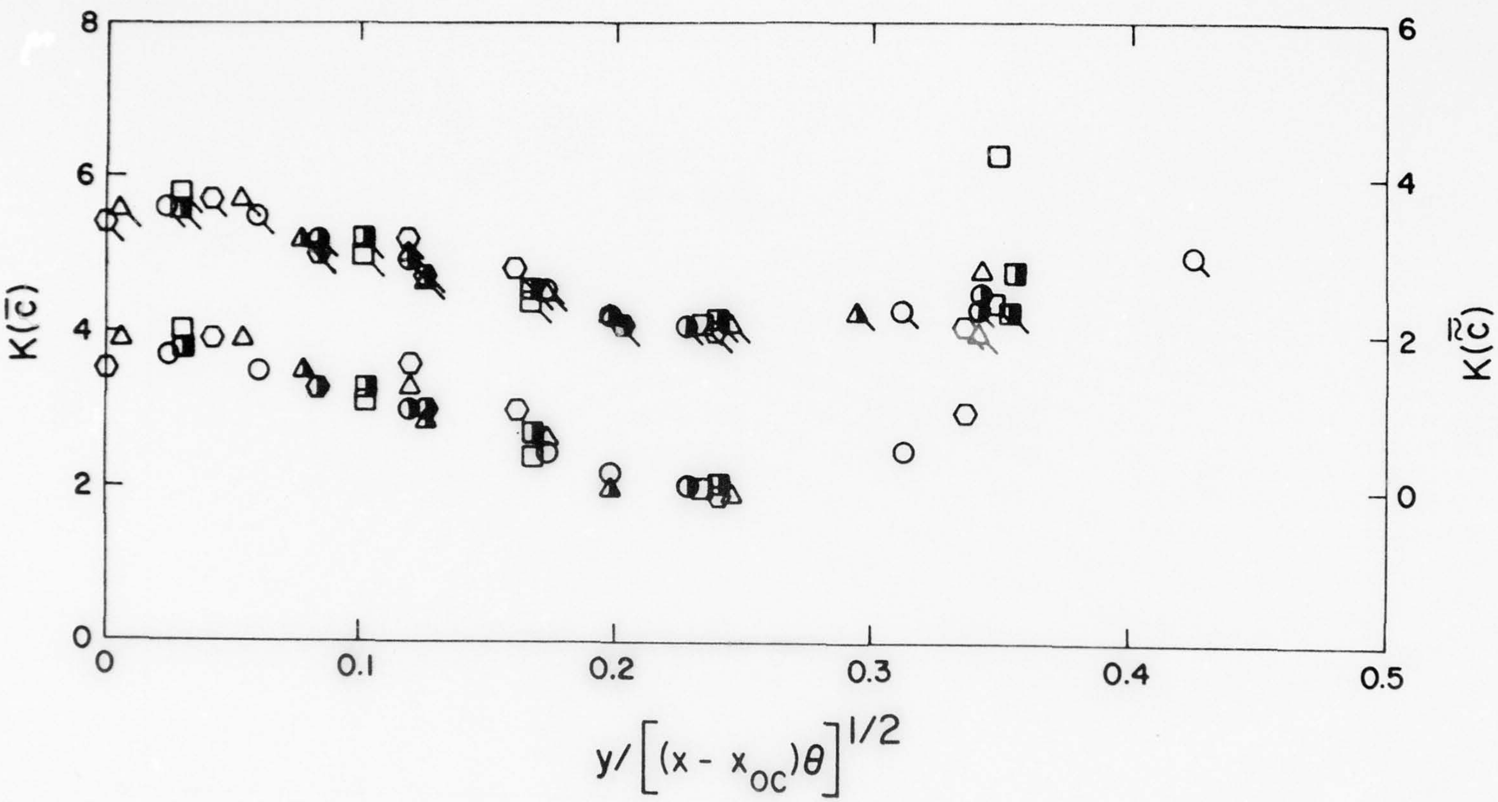

Figure 10d. Kurtosis

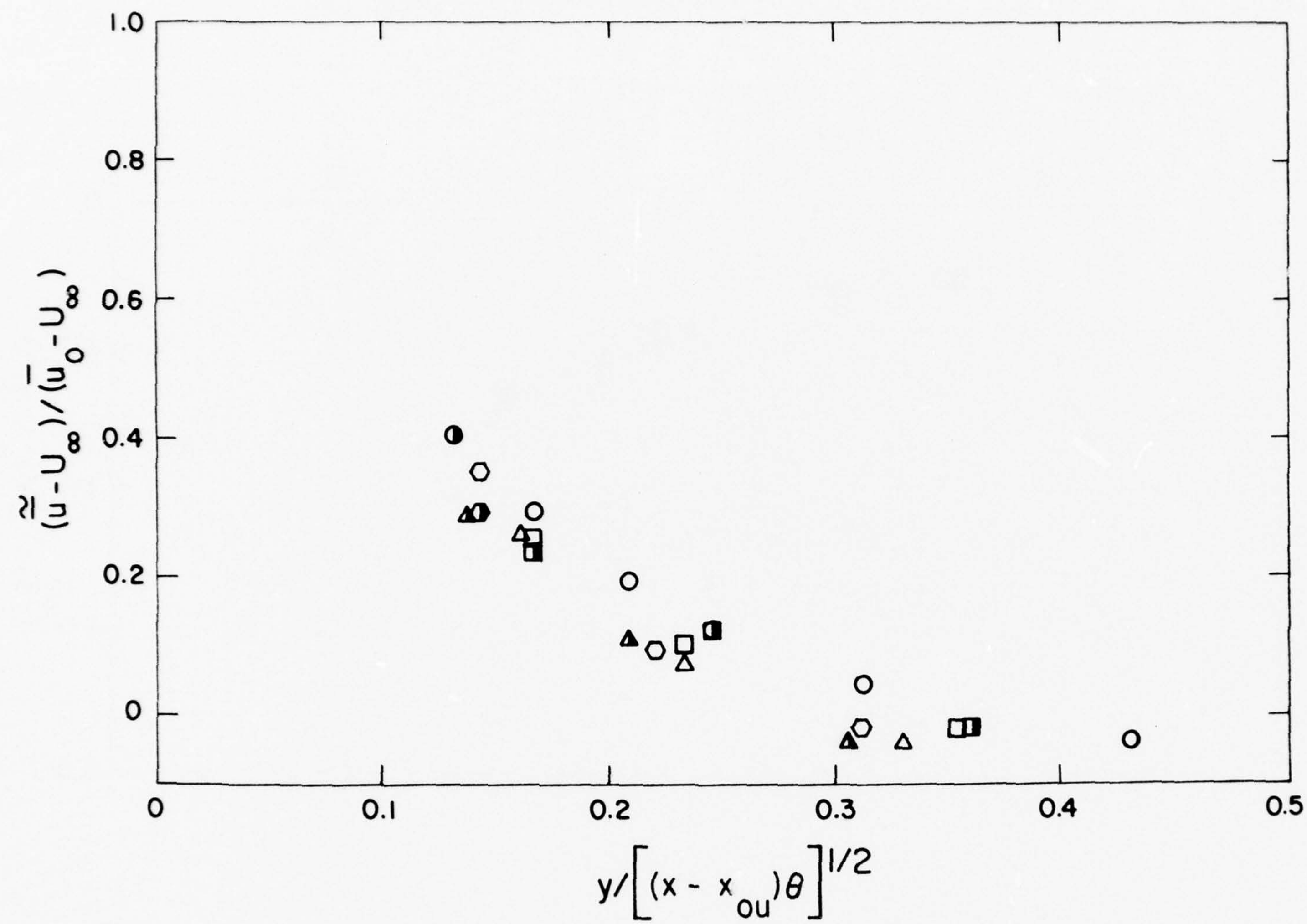

Figure 11. Irrotational zone statistics of the velocity (See Figures 7 and 9 for symbol identification) a. Mean values

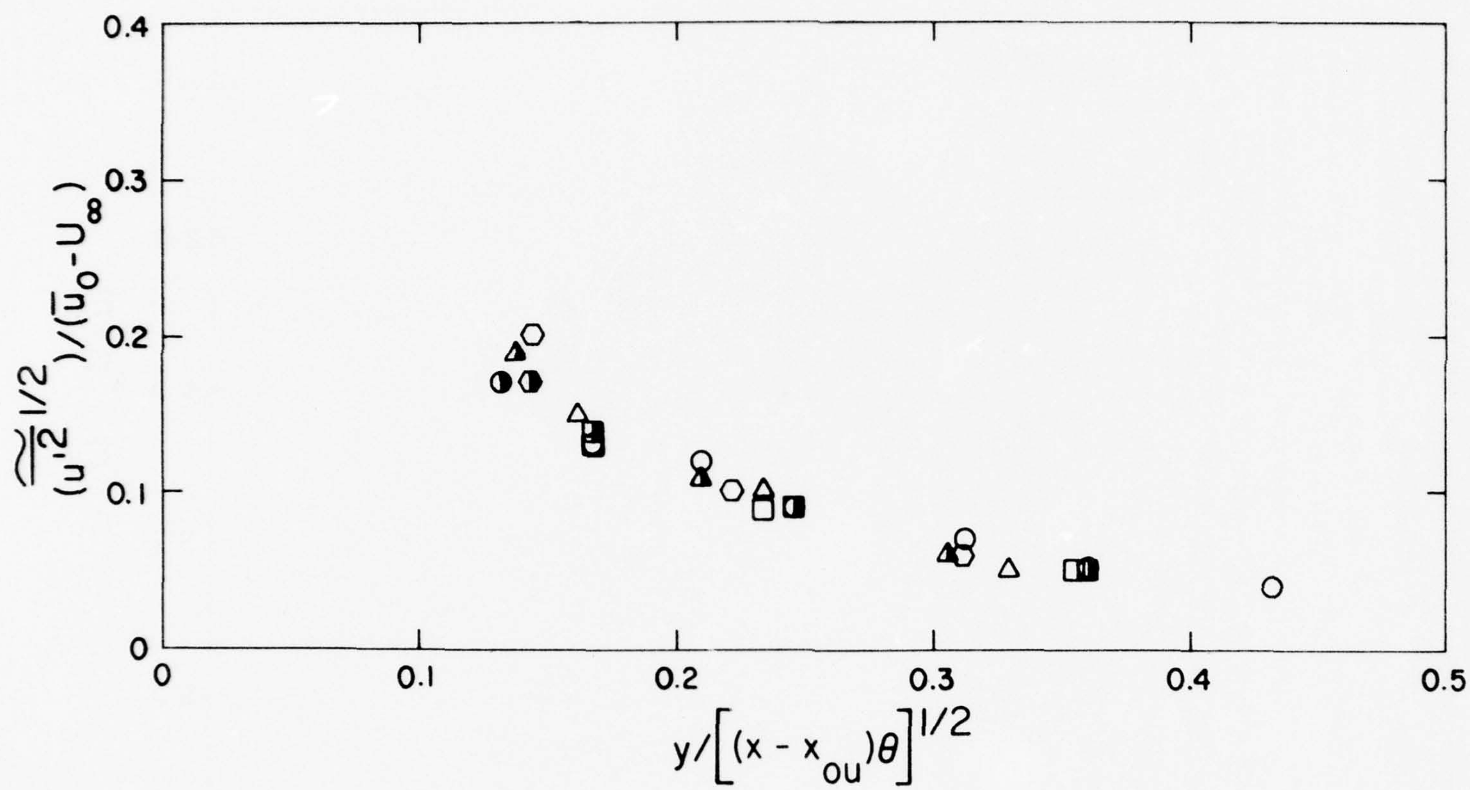

Figure 11b. Root-mean-square intensity

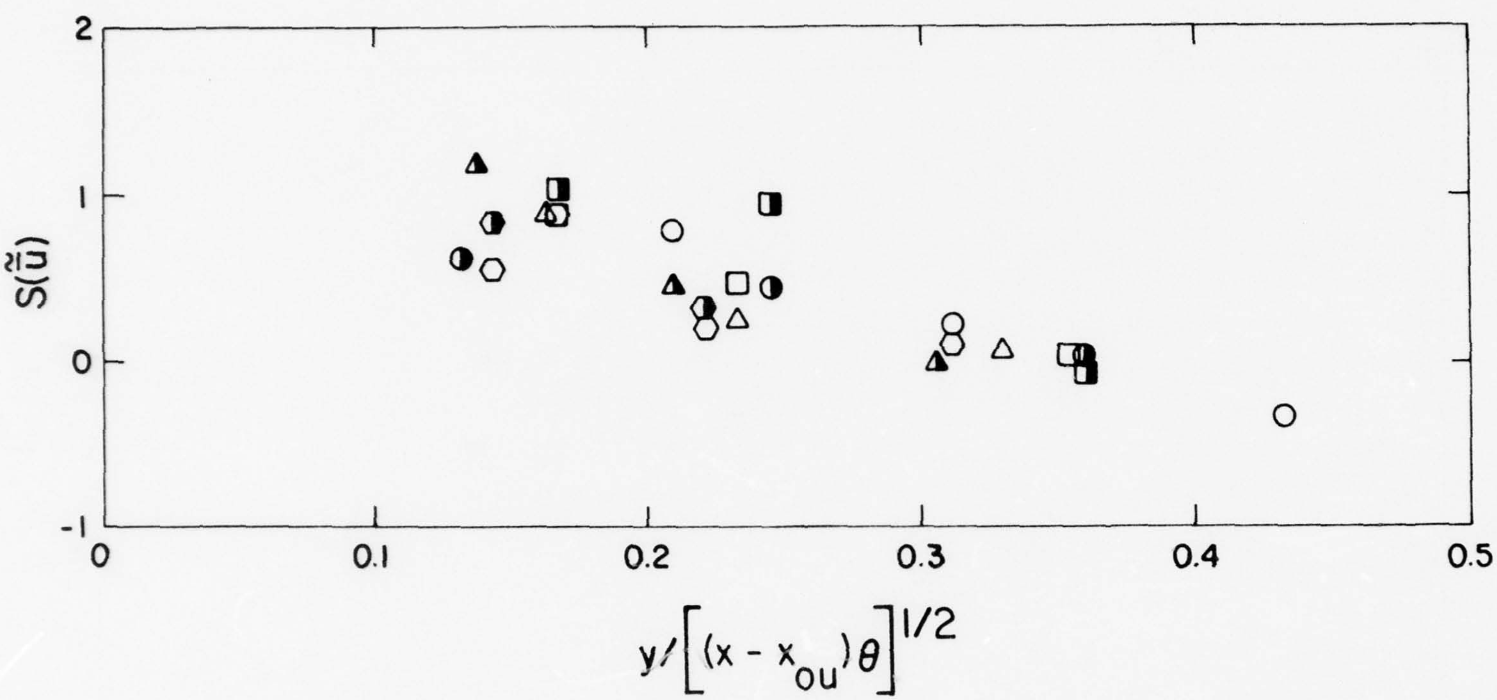

Figure 11c. Skewness

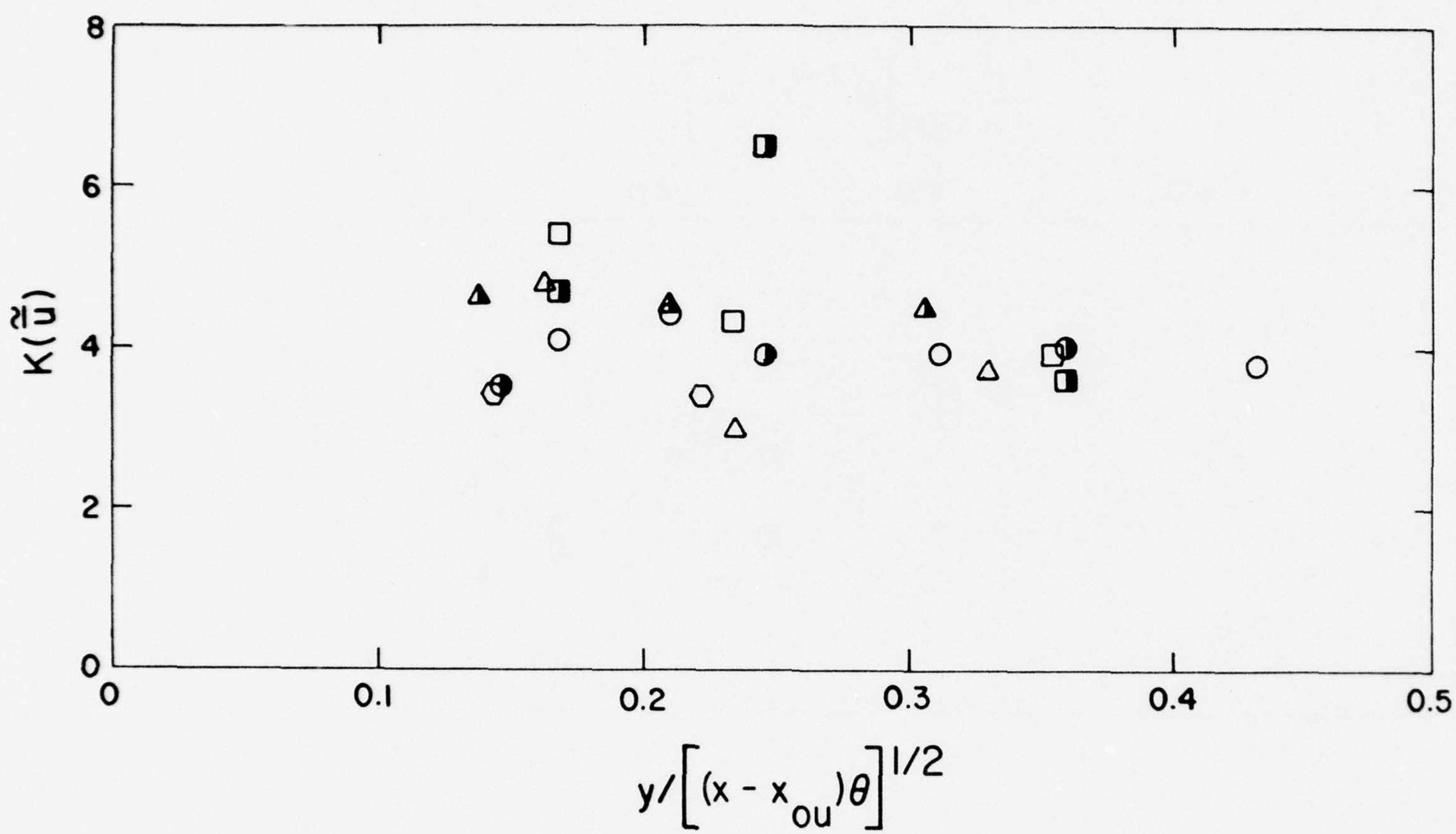

Figure 11d. Kurtosis

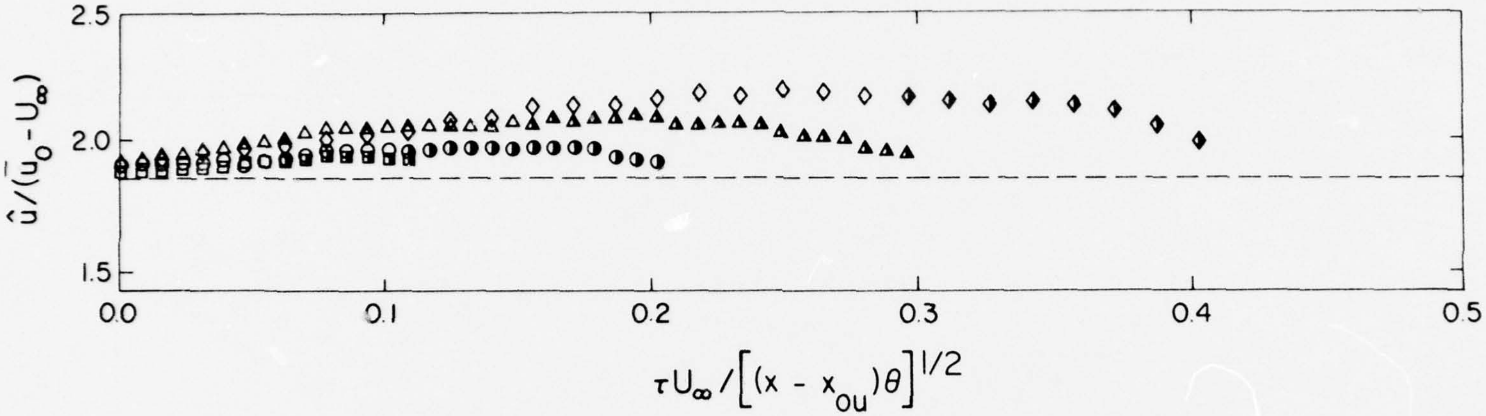

Figure 12. Range conditioned point statistics for the velocity: $\gamma = 0.846$

a. Mean values

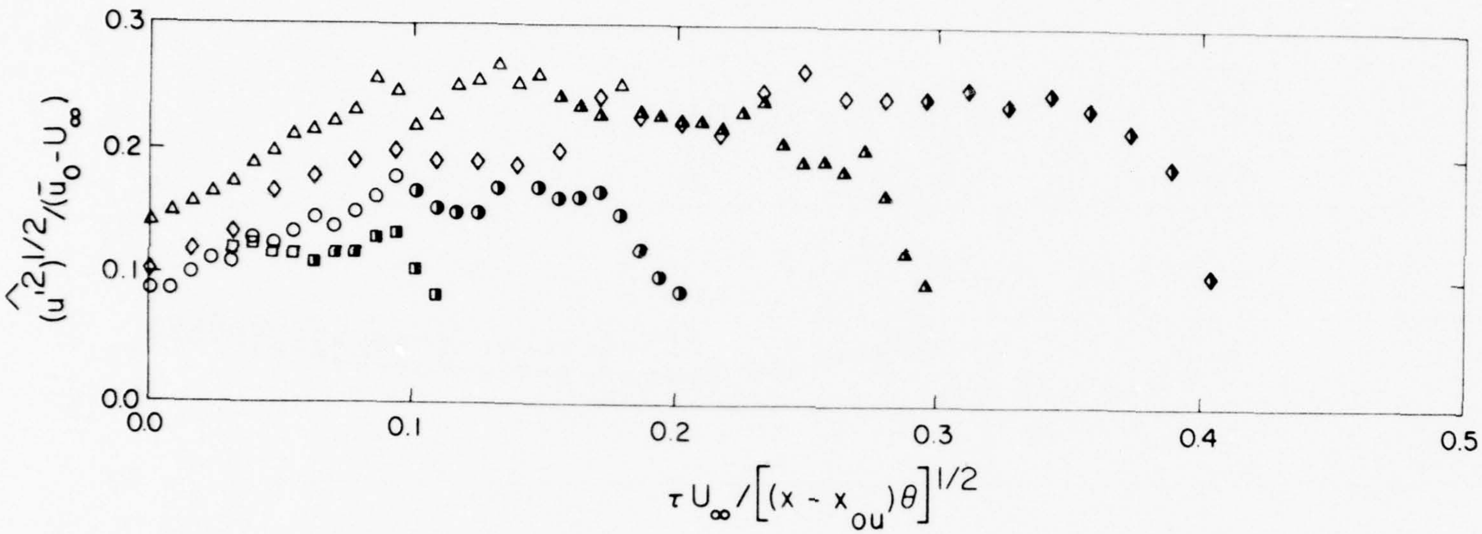

Figure 12b. Root-mean-square intensity

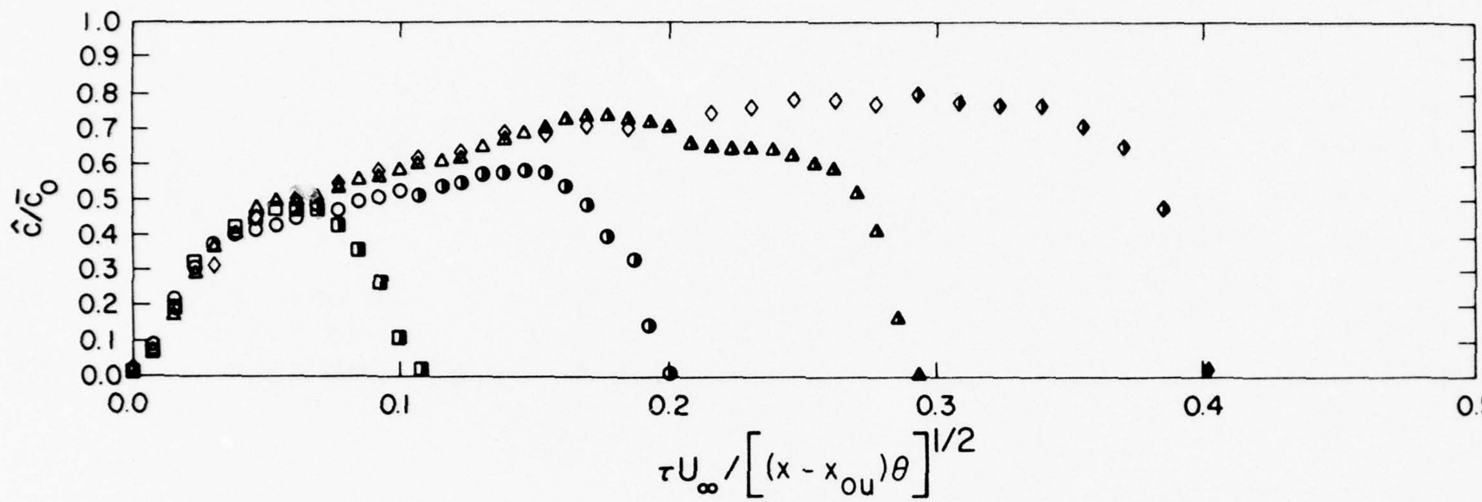

Figure 13. Range conditioned point statistics for the concentration of helium: $\gamma = 0.84$

a. Mean values

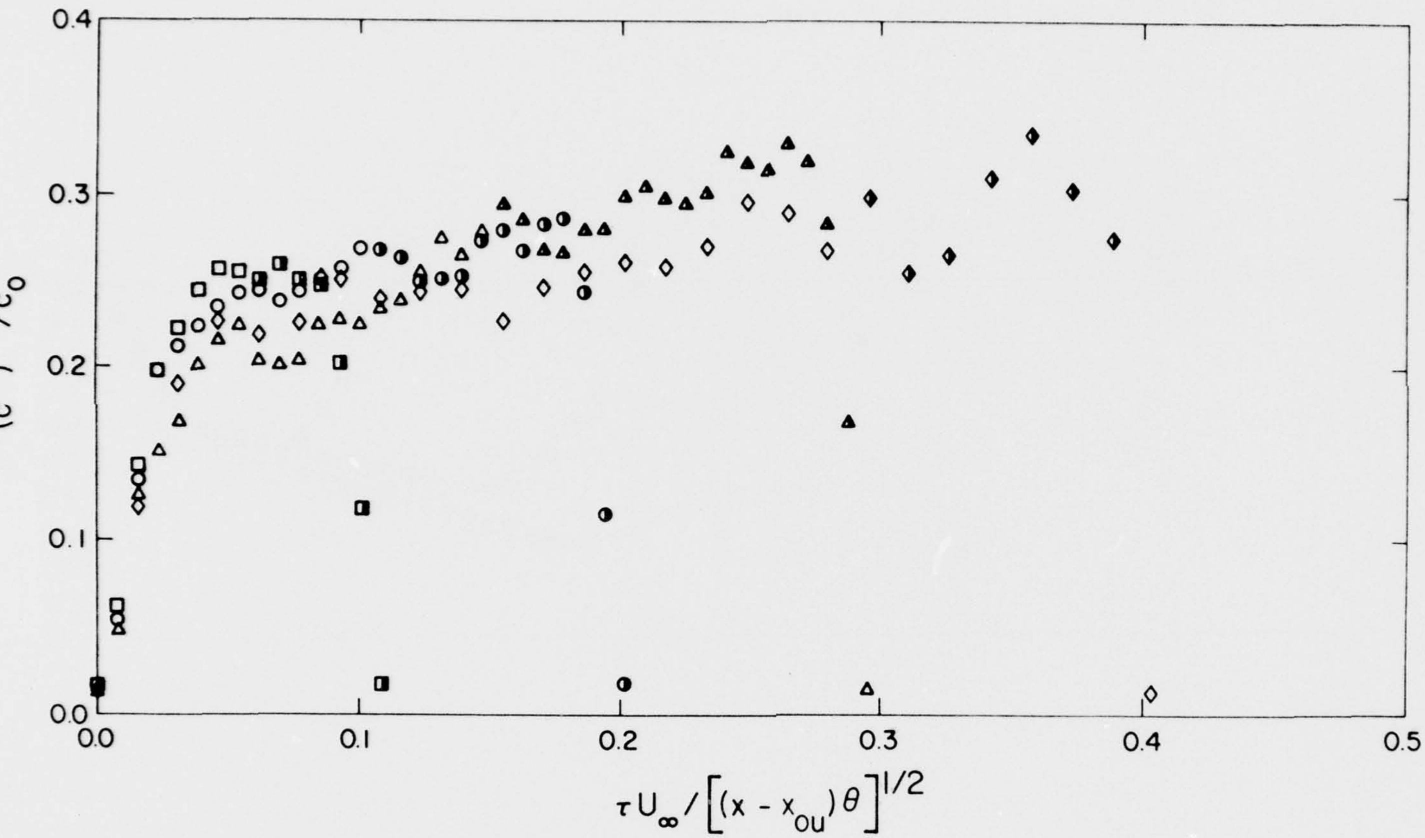

Figure 13b. Root-mean-square intensity

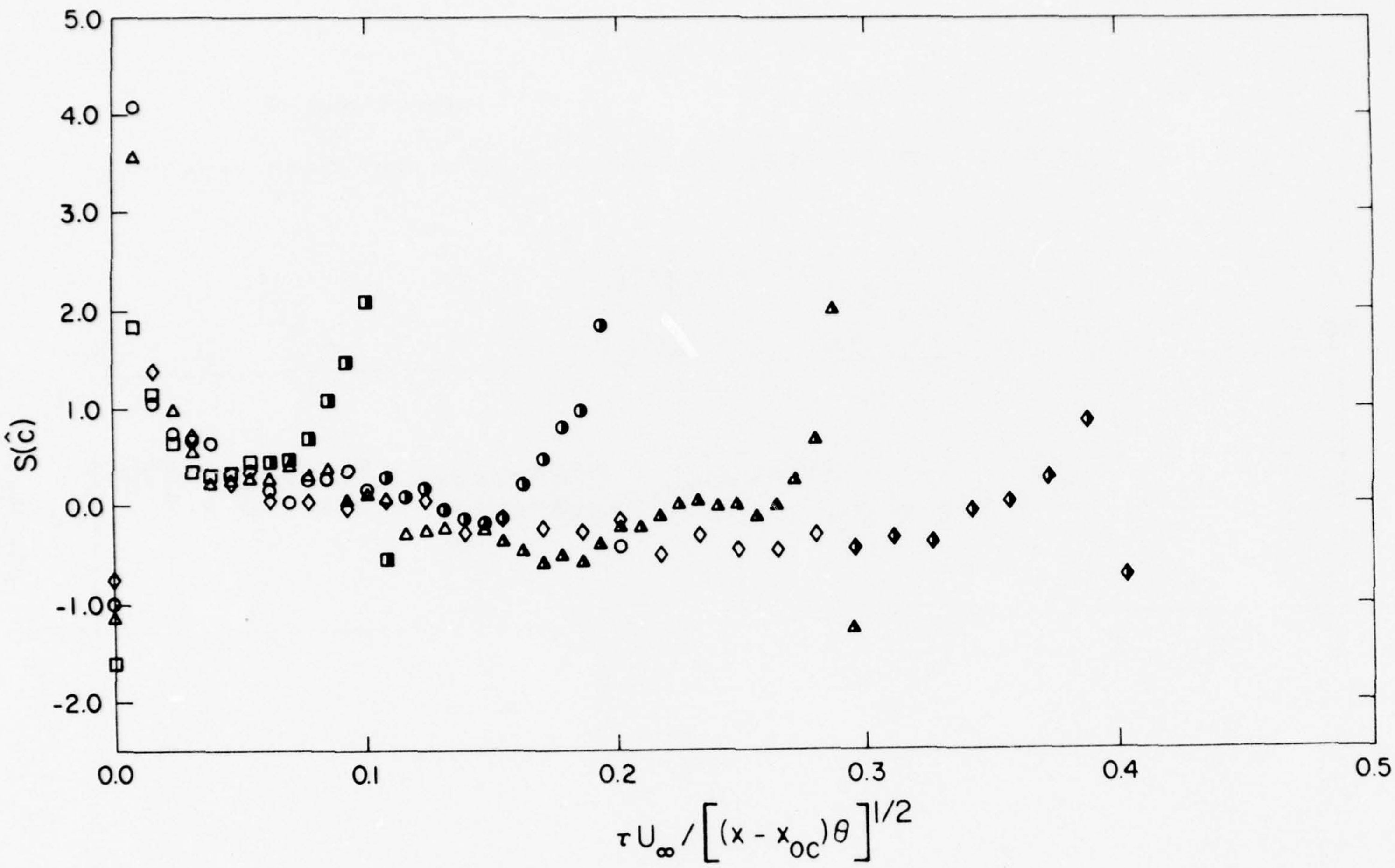

Figure 13c. Skewness

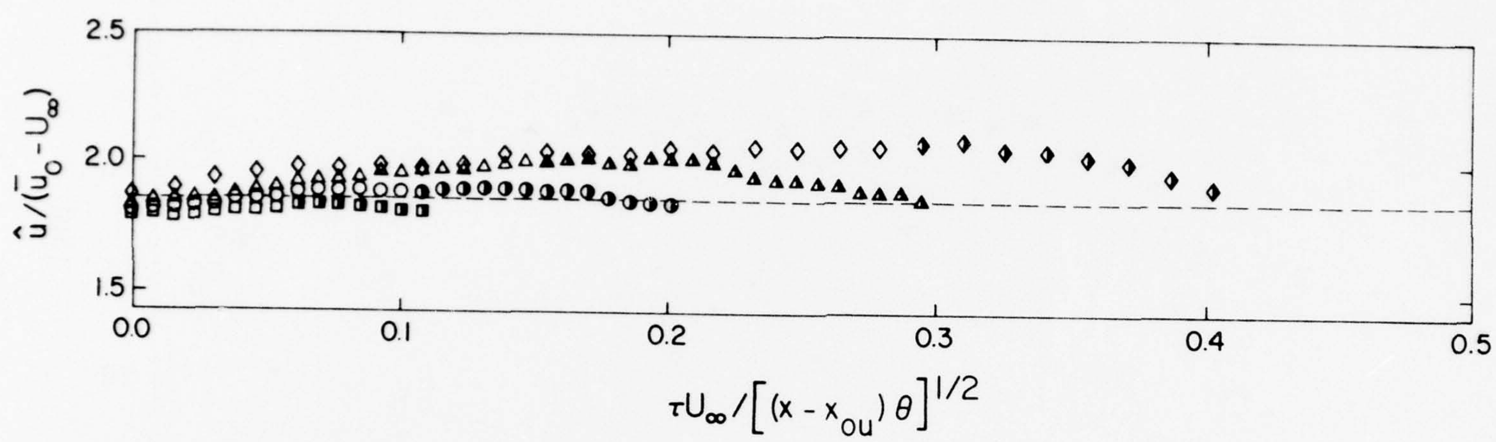

Figure 14. Range conditioned point statistics for the velocity: $\gamma = 0.34$

a. Mean values

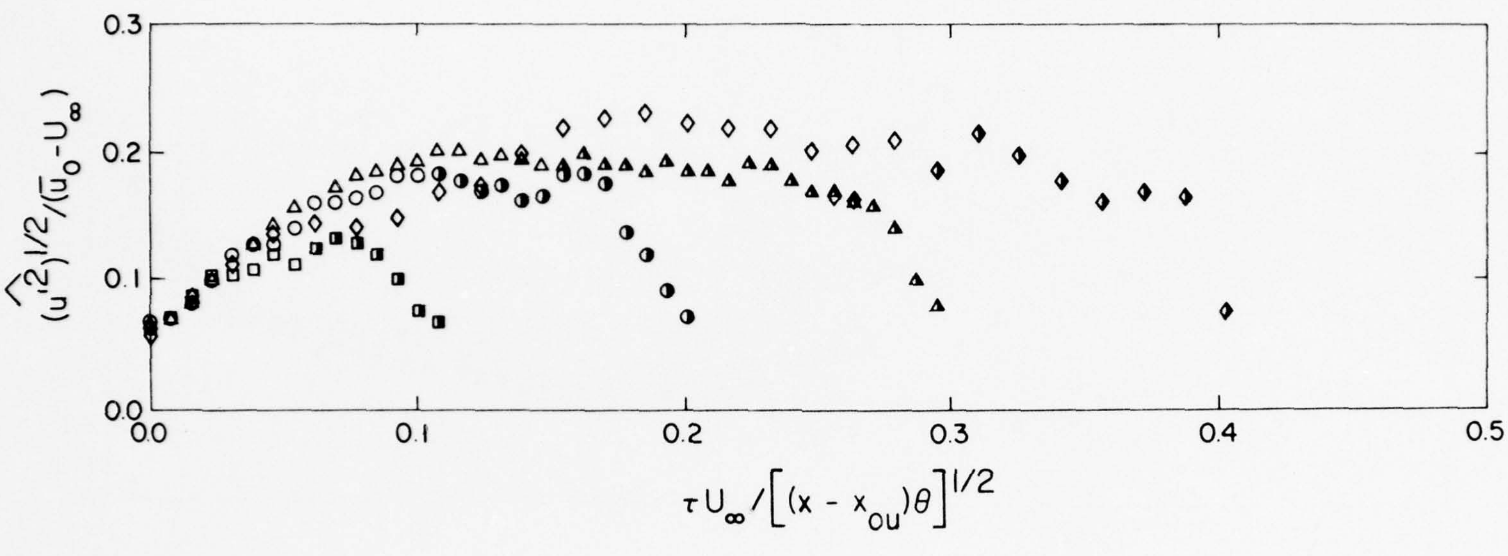

Figure 14b. Root-mean-square intensities

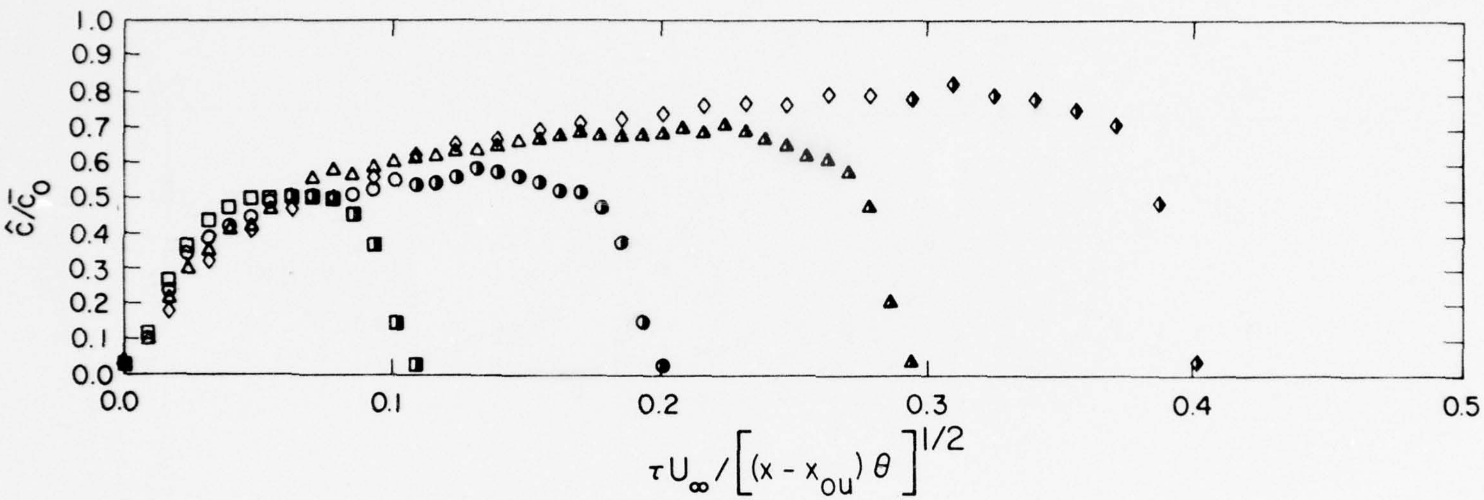

Figure 15. Range conditioned point statistics for the concentration of helium: $\gamma = 0.34$

a. Mean values

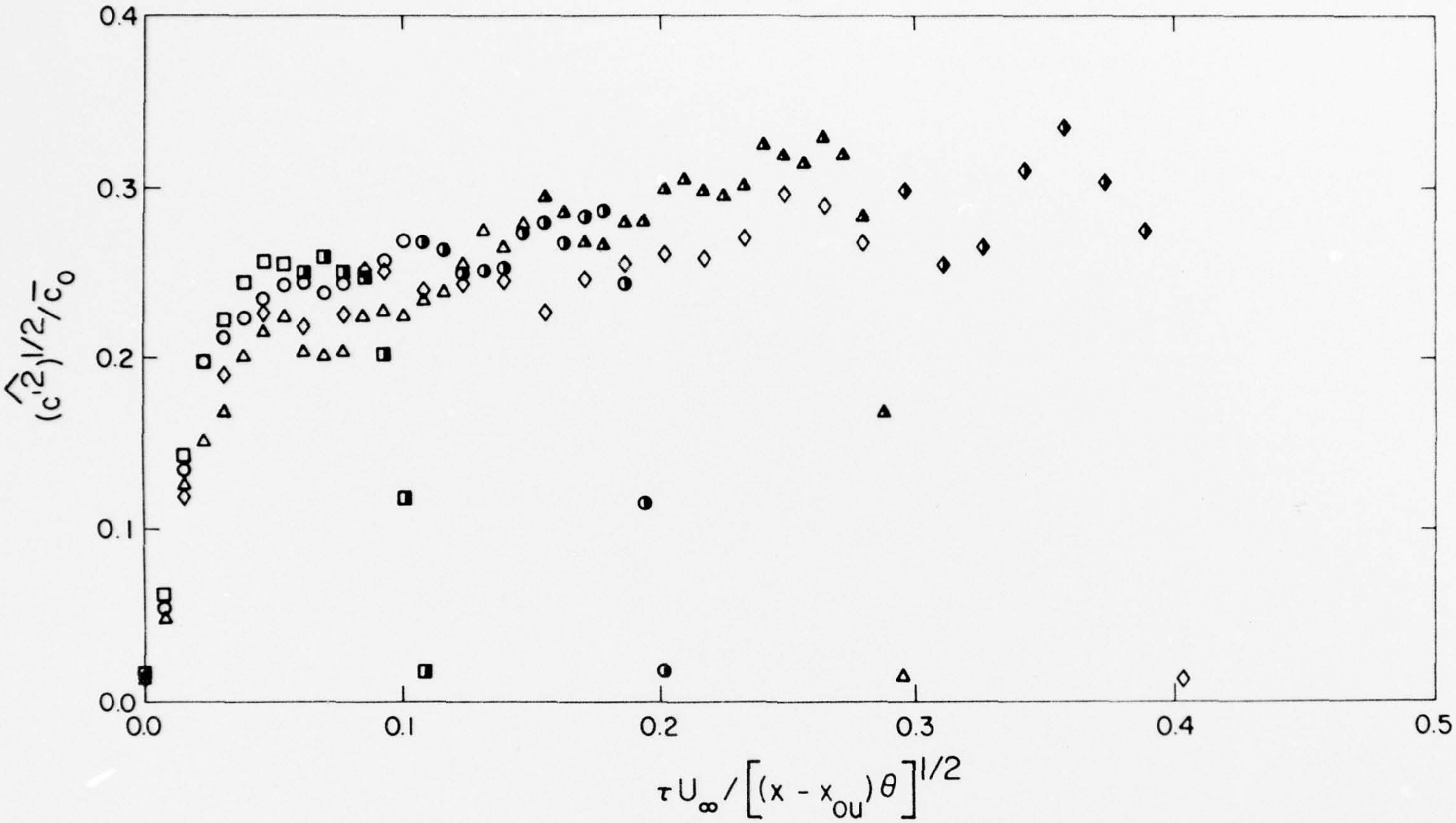

Figure 15b. Root-mean-square intensities

DISTRIBUTION LIST

GOVERNMENT AGENCIES

1. British Embassy
   3100 Massachusetts Avenue, N.W.
   Washington, D.C. 20008
   ATTN: Mr. J. Barry Jamieson
   Propulsion Officer

2. Central Intelligence Agency
   Washington, D.C. 20505
   ATTN: CRS/ADD/Publications

3. Institute for Defense Analyses
   400 Army-Navy Drive
   Arlington, Virginia 22202
   ATTN: Dr. Hans G. Wolfhard,
   Sen. Staff

4. Defense Documentation Center
   Cameron Station
   Alexandria, Virginia 22314

5. EPA Technical Center
   Research Triangle Park
   North Carolina 27711
   ATTN: Dr. W. Herget, P-222

6. Esso Research and Engineering Company
   Government Research Laboratory
   P.O. Box 8
   Linden, New Jersey 07036
   ATTN: Dr. William F. Taylor

7. Arnold Air Force Station
   Tennessee 36389
   ATTN: AEDC (DYF)

8. Arnold Air Force Station
   Tennessee 37389
   ATTN: R.E. Smith, Jr., Chief
   T-Cells Division
   Engine Test Facility

9. Air Force Aero Propulsion Laboratory
   Wright-Patterson Air Force Base
   Ohio 45433
   ATTN: STINFO Office

10. Air Force Eastern Test Range
    MU-135
    Patrick Air Force Base
    Florida 32925
    ATTN: AFETR Technical Library

11. Air Force Office of Scientific Research
    Bolling Air Force Base, Building 410
    Washington, D.C. 20332
    ATTN: Dr. Joseph F. Masi

12. Air Force Aero Propulsion Laboratory
    Wright-Patterson AFB, Ohio 45433
    ATTN: AFAPL/TBC
    Dr. Kervyn Mach

13. Air Force Aero Propulsion Laboratory
    Wright-Patterson AFB, Ohio 45433
    ATTN: AFAPL/TBC
    Francis R. Ostdiek

14. Air Force Rocket Propulsion Laboratory
    Department of Defense
    Edwards AFB, California 93523
    ATTN: LKCG (Mr. Selph)

15. U.S. Army Air Mobility Research and
    Development Laboratory
    Eustis Directorate
    Fort Eustis, Virginia 23604
    ATTN: Propulsion Division
    (SAVDL-EU-PP)

16. U.S. Army Artillery Combat
    Developments Agency
    Fort Sill, Oklahoma 73503
    ATTN: Commanding Officer

17. U.S. Army Missile Command
    Redstone Arsenal, Alabama 35809
    ATTN: AMSMI-RR

18. U.S. Army Missile Command
    Redstone Scientific Information Center
    Redstone Arsenal, Alabama 35809
    ATTN: Chief, Document Section

19. Indiana State Library
    140 North Senate Avenue
    Indianapolis, Indiana 46204
    ATTN: Patricia Matkovic
    Reference Librarian
    % Indiana Division

20. NASA Headquarters
    600 Independence
    Washington, D.C. 20546
    ATTN: Dr. Gordon Banerian

21. NASA Headquarters
    Aeronautical Propulsion Division
    Code RL, Deputy Director
    Office of Advanced Research & Technology
    Washington, D.C. 20546
    ATTN: Mr. Nelson F. Rekos

22. NASA Ames Research Center
    Deputy Chief Aeronautics Division
    Mail Stop 27-4
    Moffett Field, California 94035
    ATTN: Mr. Edward W. Perkins

23. NASA Ames Research Center
    Aerodynamics Branch 227-8
    Moffett Field, California 94305
    ATTN: Mr. Ira R. Schwartz

24. NASA Lewis Research Center
    21000 Brookpark Road
    Cleveland, Ohio 44135
    ATTN: D. Morris, Mail Stop 60-3

25. NASA Lewis Research Center
    Hypersonic Propulsion Section
    Mail Stop 6-1
    21000 Brookpark Road
    Cleveland, Ohio 44135
    ATTN: Dr. Louis A. Povinelli

26. NASA Marshall Space Flight Center
    S&E ASTN-P
    Huntsville, Alabama 35812
    ATTN: Mr. Keith Chandler

27. National Science Foundation
    Engineering Energetics
    Engineering Division
    Washington, D.C. 20550
    ATTN: Dr. George Lee

28. National Science Foundation
    Engineering Energetics
    Engineering Division
    Washington, D.C. 20550
    ATTN: Dr. M. Ojalvo

29. National Science Foundation
    Engineering Energetics
    Engineering Division
    Washington, D.C. 20550
    ATTN: Dr. Royal Rostenbach

30. Naval Air Development Center
    Commanding Officer (AD-5)
    Warminster, Pennsylvania 18974
    ATTN: NADC Library

31. Naval Air Propulsion Test Center (R&T)
    Trenton, New Jersey 08628
    ATTN: Mr. Al Martino

32. Naval Air Systems Command
Department of the Navy
Washington, D.C. 20360
ATTN: Research Administrator
AIR 310

33. Naval Air Systems Command
Department of the Navy
Washington, D.C. 20360
ATTN: Propulsion Technology Admin.
AIR 330

34. Naval Air Systems Command
Department of the Navy
Washington, D.C. 20360
ATTN: Technical Library Division
AIR 604

35. Naval Ammunition Depot
Research and Development Department
Building 190
Crane, Indiana 47522
ATTN: Mr. B.E. Douda

36. Naval Ordnance Laboratory Commander
White Oak
Silver Springs, Maryland 20910
ATTN: Library

37. Naval Ordnance Systems Command
Department of the Navy
Washington, D.C. 20360
ATTN: ORD 0331

38. Naval Postgraduate School
Department of Aeronautics, Code 57
Monterey, California 93940
ATTN: Dr. Allen E. Fuhs

39. Naval Postgraduate School
Library (Code 2124)
Monetrey, California 93940
ATTN: Superintendent

40. Naval Postgraduate School
Monterey, California 93940
ATTN: Library (Code 0212)

41. Office of Naval Research Branch Office
1030 East Green Street
Pasadena, California 91106
ATTN: Dr. Rudolph J. Marcus

42. Office of Naval Research Branch Office
536 South Clark Street
Chicago, Illinois 60605
ATTN: Commander

43. Office of Naval Research Branch Office
495 Summer Street
Boston, Massachusetts 02210
ATTN: Commander

44. Office of Naval Research
Power Branch, Code 473
Department of the Navy
Arlington, Virginia 22217

45. Office of Naval Research
Fluid Dynamics Branch, Code 438
Department of the Navy
Washington, D.C. 22217
ATTN: Mr. Morton Cooper

46. Naval Research Lab
Code 7710
Washington, D.C. 20390
ATTN: W.W. Balwanz

47. Naval Research Laboratory Director
Washington, D.C. 20390
ATTN: Technical Information Division

48. Naval Research Laboratory Director
Washington, D.C. 20390
ATTN: Library Code 2629 (ONRL)

49. Naval Ship Research and Development Center
Annapolis Division
Annapolis, Maryland 21402
ATTN: Library, Code A214

50. Naval Ship Systems Command
Department of the Navy
Washington, D.C. 20360
ATTN: Technical Library

51. Naval Weapons Center Commander
China Lake, California 93555
ATTN: Airbreathing Propulsion Branch
Code 4583

52. Naval Weapons Center
Chemistry Division
China Lake, California 93555
ATTN: Dr. William S. McEwan
Code 605

53. Naval Weapons Center
Commander
China Lake, California 93555
ATTN: Technical Library

54. Naval Weapons Center
Code 608, Thermochemistry Group
China Lake, California 93555
ATTN: Mr. Edward W. Price, Head

55. Naval Weapons Laboratory
Dahlgren, Virginia 22448
ATTN: Technical Library

56. Naval Undersea Research and
Development Center
San Diego, California 92132
ATTN: Technical Library
Code 1311D

57. Naval Underwater Systems Center
Fort Trumbull
New London, Connecticut 06320
ATTN: Technical Library

58. Naval Underwater Systems Center
Code 5B-331
Newport, Rhode Island 02840
ATTN: Dr. Robert Lazar

59. Picatinny Arsenal
Commanding Officer
Dover, New Jersey 07801
ATTN: Technical Information Library

60. State Documents Section
Exchange and Gift Division
Washington, D.C. 20540
ATTN: Library of Congress

U.S. INDUSTRIES AND LABORATORIES

61. AeroChem Research Laboratories, Inc.
P.O. Box 12
Princeton, New Jersey 08540
ATTN: Dr. Arthur Fontijn

62. AeroChem Research Laboratories, Inc.
P.O. Box 12
Princeton, New Jersey 08540
ATTN: Library

63. Aerojet Liquid Rocket Company
P.O. Box 13222
Sacramento, California 95813
ATTN: Technical Information Center

64. Aeronautical Research Association
of Princeton
50 Washington Road
Princeton, New Jersey 08540
ATTN: Dr. C. Donaldson

65. Aeroprojects, Inc.
West Chester
Pennsylvania 19380

66. The Aerospace Corporation
P.O. Box 92957
Los Angeles, California 90009
ATTN: Mr. Alexander Muraszew

67. Atlantic Research Corporation
5390 Cherokee Avenue
Alexandria, Virginia 22314
ATTN: Dr. Andrej Macek

68. Atlantic Research Corporation
5390 Cherokee Avenue
Alexandria, Virginia 22314
ATTN: Librarian

69. Atlantic Research Corporation
5390 Cherokee Avenue
Alexandria, Virginia 22314
ATTN: Dr. Kermit E. Woodcock
Manager, Propulsion

70. Avco Everett Research Laboratory
Everett, Massachusetts 02149
ATTN: Librarian

71. Avco Lycoming Corporation
550 South Main Street
Stratford, Connecticut 06497
ATTN: Mr. John W. Schrader

72. Ballistics Research Laboratory
Commanding Officer
Aberdeen Proving Ground, Maryland 21005
ATTN: Library

73. Battelle
Columbus Laboratories
505 King Avenue
Colubmus, Ohio 43201
ATTN: Mr. Abbott A. Putnam
Atmospheric Chemistry &
Combustion Systems Division

74. Beech Aircraft Corporation
9709 East Central
Wichita, Kansas 67201
ATTN: William M. Byrne, Jr.

75. Bell Aerospace Company
P.O. Box 1
Buffalo, New York 14240
ATTN: Technical Library

76. Bureau of Mines
Bartlesville Energy Research Center
Box 1398
Bartlesville, Oklahoma 74003

77. Calspan Corporation
4455 Genessee Street
Buffalo, New York 14221
ATTN: Head Librarian

78. Computer Genetics Corporation
Wakefield, Massachusetts 01880
ATTN: Mr. Donald Leonard
Technical Director

79. Convair Aerospace Division
Manager of Propulsion
P.O. Box 748
Fort Worth, Texas 76101
ATTN: L. H. Schreiber

80. Detroit Diesel Allison Division
P.O. Box 894
Indianapolis, Indiana 46206
ATTN: Dr. Sanford Fleeter

81. Dynalysis of Princeton
20 Nassau Street
Princeton, New Jersey 08540
ATTN: Dr. H.J. Herring

82. Fairchild Industries
Fairchild Republic Division
Farmingdale, New York 11735
ATTN: Engineering Library

83. Flame Research, Inc.
P.O. Box 10502
Pittsburgh, Pennsylvania 15235
ATTN: Dr. John Manton

84. Forest Fire and Engineering Research
Pacific Southwest Forest & Range
Experiment Station
P.O. Box 245
Berkeley, California 94701
ATTN: Assistant Director

85. Garrett Corporation
AiResearch Manufacturing Company
Sky Harbor Airport
402 South 36th Street
Phoenix, Arizona 85034
ATTN: Mr. Aldo L. Romanin, Mgr.
Aircraft Propulsion Engine
Product Line

86. General Dynamics
Electro Dynamic Division
P.O. Box 2507
Pomona, California 91766
ATTN: Library MZ 620

87. General Dynamics
P.O. Box 748
Fort Worth, Texas 76101
ATTN: Technical Library MZ 2246

88. General Electric Company
AEG Technical Information Center
Mail Drop N-32, Building 700
Cincinnati, Ohio 45215
ATTN: J.J. Brady

89. General Electric Company
SPO-Bldg, 174AE
1000 Western Avenue
West Lynn, Massachusetts 01910
ATTN: Mr. W. Bruce Gist

90. General Electric Space Sciences Lab
Valley Forge Space Technology Center
Room M-9144
P.O. Box 8555
Philadelphia, Pennsylvania 19101
ATTN: Dr. Theodore Baurer

91. General Motors Corporation
Detroit Diesel Allison Division
P.O. Box 894
Indianapolis, Indiana 46206
ATTN: Mr. P.C. Tram

92. General Motors Technical Center
Passenger Car Turbine Development
General Motors Engineering Staff
Warren, Michigan 48090
ATTN: T.F. Nagey, Director

93. Grumman Aerospace Corporation
Manager Space Vehicle Development
Bethpage, New York 11714
ATTN: Mr. O.S. Williams

94. Mr. Daniel L. Harshman
11131 Embassy Drive
Cincinnati, Ohio 45240

95. Hercules Incorporated
Allegany Ballistics Laboratory
P.O. Box 210
Cumberland, Maryland 21502
ATTN: Mrs. Louise S. Derrick
Librarian

96. Hercules Incorporated
P.O. Box 98
Magna, Utah 84044
ATTN: Library 100-H

97. LTV Vought Aeronautics Company
Flight Technology, Project Engineer
P.O. Box 5907
Dallas, Texas 75222
ATTN: Mr. James C. Utterback

98. Lockheed Aircraft Corporation
Lockheed Missiles and Space Company
Huntsville, Alabama 35804
ATTN: John M. Banefield
Supervisor Propulsion

99. Lockheed-Georgia Company
Dept. 72-47, Zone 259
Marietta, Georgia 30060
ATTN: William A. French

100. Lockheed Missiles and Space Company
3251 Hanover Street
Palo Alto, California 94304
ATTN: Palo Alto Library 52-52

101. Lockheed Propulsion Company
Scientific and Technical Library
P.O. Box 111
Redlands, California 92373
ATTN: Head Librarian

102. Los Alamos Scientific Laboratory
P.O. Box 1663
Los Alamos, New Mexico 97544
ATTN: J. Arthur Freed

103. The Marquardt Company
CCI Aerospace Corporation
16555 Saticoy Street
Van Nuys, California 91409
ATTN: Library

104. Martin-Marietta Corporation
P.O. Box 179
Denver, Colorado 90201
ATTN: Research Library 6617

105. Martin-Marietta Corporation
Orlando Division
P.O. Box 5837
Orlando, Florida 32805
ATTN: Engineering Library, mp-30

106. McDonnell Aircraft Company
P.O. Box 516
St. Louis, Missouri 63166
ATTN: Research & Engineering Library
Dept. 218 - Bldg. 101

107. McDonnell Douglas Corporation
Project Propulsion Engineer
Dept. 243, Bldg. 66, Level 25
P.O. Box 516
St. Louis, Missouri 63166
ATTN: Mr. William C. Paterson

108. McDonnell Douglas Astronautics Company
5301 Bolsa Avenue
Huntington Beach, California 92647
ATTN: A3-328 Technical Library

109. Nielsen Engineering and Research, Inc.
510 Clyde Avenue
Mountain View, California 94040
ATTN: Dr. Jack N. Nielsen

110. Northrop Corporation
Ventura Division
1515 Rancho Conejo Boulevard
Newbury Park, California 91230
ATTN: Technical Information Center

111. Mr. J. Richard Perrin
16261 Darcia Avenue
Encino, California 91316

112. Philco-Ford Corporation
Aeronutronic Division
Ford Road
Newport Beach, California 92663
ATTN: Technical Information Center

113. Pratt and Whitney Aircraft
Project Engineer, Advanced
Military System
Engineering Department - 2B
East Hartford, Connecticut 06108
ATTN: Mr. Donald S. Rudolph

114. Pratt and Whitney Aircraft Division
United Aircraft Company
400 South Main Street
East Hartford, Connecticut 06108
ATTN: Mr. Dana B. Waring
Manager-Product Technology

115. Pratt and Whitney Aircraft
Program Manager, Advanced
Military Engineer
Engineering Department - 2B
East Hartford, Connecticut 06108
ATTN: Dr. Robert I. Strough

116. Pratt and Whitney Aircraft
Florida Research and Development Company
P.O. Box 2691
West Palm Beach, Florida 33402
ATTN: Mr. William R. Alley
Chief of Applied Research

117. Rocket Research Corporation
11441 Willow Road
Redmond, Washington 98052
ATTN: Thomas A. Groudle

118. Rocketdyne Division
North American Rockwell
6633 Canoga Avenue
Canoga Park, California 91304
ATTN: Technical Information Center
D 596-108

119. Sandia Laboratories
P.O. Box 969
Livermore, California 94550
ATTN: Dr. Dan Hartley, Div. 8115

120. Sandia Laboratories
Livermore, California 94550
ATTN: Robert Gallagher

121. Sandia Laboratories
P.O. Box 5800
Albuquerque, New Mexico 87115
ATTN: Technical Library, 3141

122. Solar
2200 Pacific Highway
San Diego, California 92112
ATTN: Librarian

123. Standard Oil Company (Indiana)
P.O. Box 400
Naperville, Illinois 60540
ATTN: R. E. Pritz

124. Stauffer Chemical Company
Richmond, California 94802
ATTN: Dr. J. H. Morgenthaler

125. Teledyne CAE
1330 Laskey Road
Toledo, Ohio 43601
ATTN: Technical Library

126. TRW Systems
One Space Park
Redondo Beach, California 90278
ATTN: Mr. F.E. Fendell (R1/1004)

127. TRW Systems Group
One Space Park
Bldg. 0-1 Room 2080
Redondo Beach, California 90278
ATTN: Mr. Donald H. Lee Manager

128. United Technologies Research Center
East Hartford, Connecticut 06108
ATTN: Librarian

129. Valley Forge Sapce Technology Center
P.O. Box 8555
Philadelphia, Pennsylvania 19101
ATTN: Dr. Bert Zauderer

130. Vought Missiles and Space Company
P.O. Box 6267
Dallas, Texas 75222
ATTN: Library - 3-41000

U.S. COLLEGES AND UNIVERSITIES

131. Boston College
Department of Chemistry
Chestnut Hill, Massachusetts 02167
ATTN: Rev. Donald MacLean, S.J.
Associate Professor

132. Brown University
Division of Engineering
Box D
Providence, Rhode Island 02912
ATTN: Dr. R. A. Dobbins

133. California Institute of Technology
Department of Chemical Engineering
Pasadena, California 91109
ATTN: Professor W. H. Corcoran

134. California Institute of Technology
Jet Propulsion Laboratory
4800 Oak Grove Drive
Pasadena, California 91103
ATTN: Library

135. University of California, San Diego
Dept. of Engineering Physics
P.O. Box 109
La Jolla, California 92037
ATTN: Professor S.S. Penner

136. University of California
School of Engineering and
Applied Science
7513 Boelter Hall
Los Angeles, California 90024
ATTN: Engineering Reports Group

137. University of California
Lawrence Radiation Laboratory
P.O. Box 808
Livermore, California 94550
ATTN: Technical Information Dept. L-3

138. University of California
General Library
Berkeley, California 94720
ATTN: Documents Department

139. Case Western Reserve University
10900 Euclid Avenue
Cleveland, Ohio 44106
ATTN: Sears Library - Reports
Department

140. Case Western Reserve University
Division of Fluid Thermal and
Aerospace Sciences
Cleveland, Ohio 44106
ATTN: Professor Eli Reshotko

141. Colorado State University
Engineering Research Center
Fort Collins, Colorado 80521
ATTN: Mr. V. A. Sandborn

142. The University of Connecticut
Department of Mechanical Engineering
U-139
Storrs, Connecticut 06268
ATTN: Professor E. K. Dabora

143. Cooper Union
School of Engineering and Science
Cooper Square
New York, New York 10003
ATTN: Dr. Wallace Chintz
Associate Professor of ME

144. Cornell University
Department of Chemistry
Ithaca, New York 14850
ATTN: Professor Simon H. Bauer

145. Franklin Institute Research Laboratories
Philadelphia, Pennsylvania 19103
ATTN: Dr. G.P. Wachtell

146. George Washington University
Washington, D.C. 20052
ATTN: Dr. Robert Goulard
Dept. of Civil, Mechanical and
Environmental Engineering

147. George Washington University Library
Washington, D.C. 20006
ATTN: Reports Section

148. Georgia Institute of Technology
Atlanta, Georgia 30332
ATTN: Price Gilbert Memorial Library

149. Georgia Institute of Technology
School of Aerospace Engineering
Atlanta, Georgia 30332
ATTN: Dr. Ben T. Zinn

150. University of Illinois
Department of Energy Engineering
Box 4348
Chicago, Illinois 60680
ATTN: Professor Paul H. Chung

151. University of Illinois
College of Engineering
Department of Energy Engineering
Chicago, Illinois 60680
ATTN: Dr. D. S. Hacker

152. The Johns Hopkins University
Applied Physics Laboratory
Johns Hopkins Road
Laurel, Maryland 20810
ATTN: Chemical Propulsion
Information Agency

153. The Johns Hopkins University
Applied Physics Laboratory
Johns Hopkins Road
Laurel, Maryland 20810
ATTN: Document Librarian

154. The Johns Hopkins University
Applied Physics Laboratory
Johns Hopkins Road
Laurel, Maryland 20810
ATTN: Dr. A. A. Westenberg

155: University of Kentucky
Department of Mechanical Engineering
Lexington. Kentucky 40506
ATTN: Dr. Robert E. Peck

156. Massachusetts Institute of Technology
Department of Chemical Engineering
Cambridge, Massachusetts 02139
ATTN: Dr. Jack B. Howard

157. Massachusetts Institute of Technology
Libraries, Room 14 E-210
Cambridge, Massachusetts 02139
ATTN: Technical Reports

158. Massachusetts Institute of Technology
Room 10-408
Cambridge, Massachusetts 02139
ATTN: Engineering Technical Reports

159. Massachusetts Institute of Technology
Dept. of Mechanical Engineering
Room 3-350
Cambridge, Massachusetts 02139
ATTN: Dr. M. Cardillo

160. Massachusetts Institute of Technology
Dept. of Mechanical Engineering
Room 3-246
Cambridge, Massachusetts 02139
ATTN: Professor James Fay

161. Midwest Research Institute
425 Volker Boulevard
Kansas City, Missouri 64100
ATTN: Dr. T. A. Milne

162. New Mexico State University
Dept. of Mechanical Engineering
Box 3450
Las Cruces, New Mexico 88003
ATTN: Dr. Dennis M. Zallen

163. New York Institute of Technology
Wheatley Road
Old Westbury, New York 11568
ATTN: Dr. Fox

164. University of North Carolina
Periodicals and Serials Division
Drawer 870 Library
Chapel Hill, North Carolina 27514
ATTN: Mr. Stephen Berk

165. University of Notre Dame
Serials Record
Memorial Library
Notre Dame, Indiana 46556
ATTN: B. McIntosh

166. University of Notre Dame
College of Engineering
Notre Dame, Indiana 46556
ATTN: Dr. Stuart T. McComas
Assistant Dean for Research
and Special Projects

167. Ohio State University
Dept. of Chemical Engineering
140 West 19th Avenue
Columbus, Ohio 43210
ATTN: Dr. Robert S. Brodkey

168. The Pennsylvania State University
Room 207, Old Main Building
University Park, Pennsylvania 16802
ATTN: Office of Vice President
for Research

169. Princeton University
Dept. of Aerospace and Mechanical
Sciences
James Forrestal Campus
Princeton, New Jersey 08540
ATTN: Dr. Martin Summerfield

170. Princeton University
James Forrestal Campus Library
P.O. Box 710
Princeton, New Jersey 08540
ATTN: V. N. Simosko, Librarian

171. Rice University
Welch Professor of Chemistry
Houston, Texas 77001
ATTN: Dr. Joseph L. Franklin

172. University of Rochester
Dept. of Chemical Engineering
Rochester, New York 14627
ATTN: Dr. John R. Ferron

173. Stanford University
Dept. of Aeronautics and Astronautics
Stanford, California 94305
ATTN: Dr. Walter G. Vincenti

174. State University of New York - Buffalo
Dept. of Mechanical Engineering
228 Parker Engineering Building
Buffalo, New York 14214
ATTN: Dr. George Rudinger

175. Stevens Institute of Technology
Department of Mechanical Engineering
Castle Point Station
Hoboken, New Jersey 07030
ATTN: Professor Fred Sisto

176. University of Virginia
Department of Aerospace Engineering
School of Engineering and Applied Science
Charlottesville, Virginia 22901
ATTN: Dr. John E. Scott

177. University of Virginia
Science/Technology Information Center
Charlottesville, Virginia 22901
ATTN: Dr. Richard H. Austin

178. Yale University
Mason Laboratory
9 Hillhouse Avenue
New Haven, Connecticut 06520
ATTN: Professor Peter P. Wegener

FOREIGN INSTITUTIONS

179. A/S Kongsberg Vaapenfabrikk
Gas Turbine Division
3601 Konsber, NORWAY
ATTN: R.E. Stanley
Senior Aerodynamicist

180. Conservatoire National des Arts
et Metiers
292, Rue Saint'Martin
75141 Paris Cedex 03, FRANCE
ATTN: Professor J. Gossee
Chaire de Thermique

181. DFVLR-Forschungszentrum Gottingen
Institut Fur Stromungsmechanik
Abteilung Theoretische Gashynamik
D-3400 Gottingen
Bunsenstrabe 10, GERMANY
ATTN: Professor Klaus Oswatitsch

182. Ecole Royale Militaire
30 Avenue de la Resaissance
Bruxelles B-1040, BELGIUM
ATTN: Professor Emile Tits

183. Fysisch Laboratorium
Fijksuniversiteit Utrecht
Sorbonnelaan, Utrecht,
THE NETHERLANDS
ATTN: Dr. F. Van der Valk

184. Imperial College
Department of Chemical Engineering
London SW7, ENGLAND
ATTN: Professor F. J. Weinberg

185. Imperial College of Science
and Technology
Department of Mechanical Engineering
Exhibition Road
London, SW7, ENGLAND
ATTN: Professor Gaydon

186. Imperial College of Science
and Technology
Department of Mechanical Engineering
Exhibition Road
London SW7, ENGLAND
ATTN: D. B. Spalding

187/1 Laboratoire de Mecanique des Fluides
36, Route de Dardilly, 36
B.P. No. 17
69130 Ecully, FRANCE
ATTN: G. Assassa

187/2 Laboratoire de Mecanique des Fluides
Ecole Centrale Lyonnaise
36, Route de Dardilly
69130 Ecully, FRANCE
ATTN: Dr. K. Papiliou

188. Ministry of Defense
Main Building, Room 2165
Whitehall Gardens
London SW1, ENGLAND
ATTN: Mr. L.D. Nicholson ED, idc
Vice Controller of Aircraft
Procurement Executive

189. Mitglied des Vorstands der Fried
Krumpp CmbH
43 Essen, Altendorferstrabe 103
GERMANY
ATTN: Professor Dr.-Ing.
Wilhelm Dettmering

190. National Aerospace (NLR)
Voorsterweg 31
Noord-Oost-Polder-Emmelord
THE NETHERLANDS
ATTN: Mr. F. Jaarsma

191. National Research Council
Division of Mechanical Engineering
Montreal Road, Ottawa
Ontario, CANADA KIA OR6
ATTN: Dr. R.B. Whyte

192. Nissan Motor Co., LTD.
3-5-1, Momoi, Suginami-Ku
Tokyo, JAPAN 167
ATTN: Dr. Y. Toda

193. Norweigian Defense Research Establishment
Superintendent NDRE
P.O. Box 25
2007 Kjeller, NORWAY
ATTN: Mr. T. Krog

194. ONERA
Energie and Propulsion
29 Avenue de la Division Leclure
92 Chatillon sous Bagneux, FRANCE
ATTN: Mr. M. Barrere

195. ONERA
Energie and Propulsion
29 Avenue de la Division Leclure
92 Chatillon sous Bagneux, FRANCE
ATTN: Mr. J. Fabri

196. ONERA
Energie and Propulsion
29 Avenue de la Division Leclure
92 Chatillon sous Bagneux, FRANCE
ATTN: Mr. Viaud

197. ONERA-DED
External Relations and Documentation
Department
29, Avenue de la Division Leclure
92320 Chatillon, sous Bagneux, FRANCE
ATTN: Mr. M. Salmon

198. Orta Dogu Teknik Universities
Mechanical Engineering Department
Ankara, TURKEY
ATTN: Professor H. Sezgen

199. Queen Mary College
Department of Mechanical Engineering
Thile Eld Road
London E1, ENGLAND
ATTN: Professor M. W. Thring

200. Rolls-Royce (1971) Limited
Derby Engine Division
P.O. Box 31
Derby DE2 8BJ
London, ENGLAND
ATTN: C. Freeman, Installation
Research Department

201. Rome University
Via Bradano 28
00199 Rome, ITALY
ATTN: Professor Gaetano Salvatore

202. Sener
Departamentao de Investigation
Km. 22.500 de la antigua carretera
Madrid - Barcelona, SPAIN
ATTN: Mr. J. T. Diez Roche

203. Service Technique Aeronautique Moteurs
4 Avenue de la Parte d'Issy
75753 Paris Cedex 15, FRANCE
ATTN: Mr. M. Pianko, Ing. en chef

204. The University of Sheffield
Dept. of Chemical Engineering
and Fuel Technology
Mappin Street, Sheffield S1 3JD
ENGLAND
ATTN: Dr. Norman Chigier

205. Sophia University
Science and Engineering Faculty
Kioi 7 Tokyo-Chiyoda JAPAN 102
ATTN: Professor M. Susuki

206. The University of Sydney
Dept. of Mechanical Engineering
N.S.W. 2006
Sydney, AUSTRALIA
ATTN: Professor R. W. Bilger

207. Technical University of Denmark
Fluid Mechanics Department
Building 404 2800 Lyngby
DK-DENMARK
ATTN: Professor K. Refslund

208. University of Leeds
Leeds, ENGLAND
ATTN: Professor Dixon-Lewis

209. Universite de Poitiers Laboratoire
D'energetique et de Detonique
(L.A. au C.N.R.S. No. 193)
ENSMA - 86034 Poitiers, FRANCE
ATTN: Professor N. Manson

210. University of Tokyo
Department of Reaction Chemistry
Faculty of Engineering
Bunkyo-ku
Tokyo, JAPAN 113
ATTN: Professor T. Hikita

211. Vrije Universiteit Brussel
Fac. Toeg. Wetenshch.
A. Buyllaan 105
1050 Brussels, BELGIUM
ATTN: Ch. Hirsch

PROJECT SQUID CONTRACTORS
1975-76 and 1976-77 (New)

212. AeroChem Research Laboratory, Inc.
Reaction Kinetics Group
P.O. Box 12
Princeton, New Jersey 08540
ATTN: Dr. Arthur Fontijn

213. Aeronautical Research Associates of
Princeton, Inc.
P.O. Box 2229
50 Washington Road
Princeton, New Jersey 08540
ATTN: Dr. Ashok K. Varma

214. California Institute of Technology
Div. of Engineering and
Applied Science
Mail Stop 205-50
Pasadena, California 91109
ATTN: Dr. Anatol Roshko

215. Case Western Reserve University
Div. of Fluid, Thermal and Aerospace
Sciences
Cleveland, Ohio 44106
ATTN: Dr. J.S. T'ien

216. Colorado State University
Engineering Research Center
Foothills Campus
Fort Collins, Colorado 80521
ATTN: Dr. Willy Z. Sadeh

217. General Electric Company
Corporate Research and Development
P.O. Box 8
Schenectady, New York 12301
ATTN: Dr. Marshall Lapp

218. Massachusetts Institute of Technology
Chemistry Department, Room 6-123
77 Massachusetts Avenue
Cambridge, Massachusetts 02139
ATTN: Dr. John Ross

219. Michigan State University
Department of Mechanical Engineering
East Lansing, Michigan 48824
ATTN: Dr. John Foss

220. Pennsylvania State University
Applied Research Laboratory
University Park, Pennsylvania 16802
ATTN: Dr. Edgar P. Bruce

221. Polytechnic Institute of New York
Department of Aerospace Engineering
and Applied Mechanics
Farmingdale, New York 11735
ATTN: Dr. Samuel Lederman

222. Southern Methodist University
Thermal and Fluid Sciences Center
Institute of Technology
Dallas, Texas 75275
ATTN: Dr. Roger L. Simpson

223. Stanford University
Mechanical Engineering Department
Stanford, California 94305
ATTN: Dr. James P. Johnston

224. Stanford University
Mechanical Engineering Department
Stanford, California 94305
ATTN: Dr. S. J. Kline

225. Stanford University
Mechanical Engineering Department
Stanford, California 94305
ATTN: Dr. Sidney Self

226. TRW Systems
Engineering Sciences Laboratory
One Space Park
Redondo Beach, California 90278
ATTN: Dr. J. E. Broadwell

227. United Technologies Research Center
400 Main Street
East Hartford, Connecticut 06108
ATTN: Mr. Franklin O. Carta

228. United Technologies REsearch Center
400 Main Street
East Hartford, Connecticut 06108
ATTN: Dr. Alan C. Eckbreth

229. University of California - San Diego
Department of Aerospace and
Mechanical Engineering
La Jolla, California 92037
ATTN: Dr. Paul Libby

230. University of Colorado
Department of Aerospace
Engineering Sciences
Boulder, Colorado 80304
ATTN: Dr. Mahinder S. Uberoi

231. University of Michigan
Department of Aerospace Engineering
Ann Arbor, Michigan 48105
ATTN: Dr. T. C. Adamson, Jr.

232. University of Michigan
Department of Aerospace Engineering
Ann Arbor, Michigan 48105
ATTN: Dr. Martin Sichel

233. University of Missouri - Columbia
Department of Chemistry
Columbia, Missouri 65201
ATTN: Dr. Anthony Dean

234. University of Southern California
Department of Aerospace Engineering
University Park
Los Angeles, California 90007
ATTN: Dr. F. K. Browand

235. University of Washington
Department of Mechanical Engineering
Seattle, Washington 98195
ATTN: Dr. F.B. Gessner

236. Virginia Polytechnic Institute and
State University
Mechanical Engineering Department
Blacksburg, Virginia 24601
ATTN: Dr. Walter F. O'Brien, Jr.

237. Virginia Polytechnic Institute and
State University
Mechanical Engineering Department
Blacksburg, Virginia 24061
ATTN: Dr. Hal L. Moses

238. Yale University
Engineering and Applied Science
Mason Laboratory
New Haven, Connecticut 06520
ATTN: Dr. John B. Fenn

PURDUE UNIVERSITY

239. School of Aeronautics and Astronautics
Grissom Hall
West Lafayette, Indiana 47907
ATTN: Library

240. School of Mechanical Engineering
Mechanical Engineering Building
West Lafayette, Indiana 47907
ATTN: Library

241-250. Purdue University Advisors

Unclassified

SECURITY CLASSIFICATION OF THIS PAGE (When Data Entered)

REPORT DOCUMENTATION PAGE

READ INSTRUCTIONS BEFORE COMPLETING FORM

1. REPORT NUMBER	2. GOVT ACCESSION NO.	3. RECIPIENT'S CATALOG NUMBER
UCSD-9-PU		

4. TITLE (and Subtitle)

TURBULENCE MEASUREMENTS OF A TWO-DIMENSIONAL HELIUM JET IN A MOVING AIRSTREAM

5. TYPE OF REPORT & PERIOD COVERED

6. PERFORMING ORG. REPORT NUMBER

7. AUTHOR(s)

Paul Anderson, John C. LaRue, and Paul A. Libby

8. CONTRACT OR GRANT NUMBER(s)

N00014-75-C-1143

9. PERFORMING ORGANIZATION NAME AND ADDRESS

Department of Applied Mechanics and Engineering Sciences U03617
University of California, San Diego, LaJolla, CA

10. PROGRAM ELEMENT, PROJECT, TASK AREA & WORK UNIT NUMBERS

NR-098-038

11. CONTROLLING OFFICE NAME AND ADDRESS

Project SQUID, Chaffee Hall
Purdue University
West Lafayette, Indiana 47907

12. REPORT DATE

June 1977

13. NUMBER OF PAGES

77

14. MONITORING AGENCY NAME & ADDRESS (if different from Controlling Office)

Office of Naval Research
Department of the Navy
Arlington, Virginia 22217

15. SECURITY CLASS. (of this report)

Unclassified

15a. DECLASSIFICATION/DOWNGRADING SCHEDULE

16. DISTRIBUTION STATEMENT (of this Report)

This document has been approved for public release and sale; its distribution is unlimited.

17. DISTRIBUTION STATEMENT (of the abstract entered in Block 20, if different from Report)

18. SUPPLEMENTARY NOTES

19. KEY WORDS (Continue on reverse side if necessary and identify by block number)

Turbulence
Jets
Intermittency
Conditioned sampling
Passive scalars
Hot-wire anemometry
Entrainment

20. ABSTRACT (Continue on reverse side if necessary and identify by block number)

Measurements of the streamwise velocity component and the concentration of helium are made in a two-dimensional helium jet discharging into a moving airstream. The transverse distribution of the unconditioned and conditioned statistics of the velocity and helium concentration at various downstream positions are presented. In addition range conditioned point statistics provide information on the structure of turbulent zones of various durations.

The gross properties of the jet agree with previous data. Entrainment is found to occur on the leeward edges of the turbulent zones; because the → next Page

DD FORM 1 JAN 73 1473 EDITION OF 1 NOV 65 IS OBSOLETE

S/N 0102-014-6601

Unclassified

SECURITY CLASSIFICATION OF THIS PAGE (When Data Entered) turbulent fluid is moving faster than the external stream these edges are on the upstream end of the zones. The interfaces as given by the velocity and concentration cannot be distinguished and are found to be relatively thicker than previously measured temperature interfaces.